



Published in final edited form as:

Nat Metab. 2020 December ; 2(12): 1413–1426. doi:10.1038/s42255-020-00313-3.

An Enolase Inhibitor for the Targeted Treatment of *ENO1*-Deleted Cancers

Yu-Hsi Lin¹, Nikunj Satani^{1,2}, Naima Hammoudi¹, Victoria C. Yan¹, Yasaman Barekatin¹, Sunada Khadka¹, Jeffrey J. Ackroyd¹, Dimitra K. Georgiou¹, Cong-Dat Pham¹, Kenisha Arthur¹, David Maxwell³, Zhenghong Peng⁴, Paul G. Leonard^{5,6}, Barbara Czako⁶, Federica Pisaneschi¹, Pijus Mandal⁶, Yuting Sun⁶, Rafal Zielinski⁷, Susana Castro Pando¹, Xiaobo Wang¹, Theresa Tran¹, Quanyu Xu⁸, Qi Wu⁸, Yongying Jiang⁸, Zhijun Kang⁶, John M. Asara⁹, Waldemar Priebe⁷, William Bornmann¹⁰, Joseph R. Marszalek¹¹, Ronald A. DePinho¹², Florian L. Muller^{1,*}

¹Department of Cancer Systems Imaging, University of Texas MD Anderson Cancer Center, Houston, TX 77054

²Institute of Stroke and Cerebrovascular Disease, University of Texas Health Science Center at Houston, TX 77030

³Institutional Analytics & Informatics, University of Texas MD Anderson Cancer Center, Houston, TX 77030

⁴Cardtronics, Inc., Houston, TX 77042

Users may view, print, copy, and download text and data-mine the content in such documents, for the purposes of academic research, subject always to the full Conditions of use:http://www.nature.com/authors/editorial_policies/license.html#terms

*Correspondence should be addressed to Florian L. Muller, Department of Cancer Systems Imaging, University of Texas MD Anderson Cancer Center, Houston, TX 77054; aettius@aol.com.

AUTHOR CONTRIBUTIONS.

F.L.M. and D.M. conceived HEX and POMHEX, which were synthesized by Z.P. and W.B. Z.K., F.P., P.M., B.C., C-D.P, V.C.Y., and F.L.M. repeated chemical syntheses; V.C.Y., B.C., and F.L.M. wrote synthetic procedures with characterizations. N.S. and F.L.M. performed *in vitro* enzymatic activity inhibitor experiments. P.G.L. performed isolation of ENO2 recombinant protein and X-ray crystallography with HEX. R.Z. and W.P. performed Seahorse experiments. N.H., N.S., S.K., S.C.P., X.W., T.T., and K.A. performed cell culture Enolase inhibitor sensitivity testing. J.J.A. performed western blots. Y.B. performed in NMR experiments. Y-H.L. and F.L.M. performed ¹³C-NMR tracing and biochemical profiling experiments. J.M.A. performed mass spectrometry and small molecule metabolite analysis. Q.X., Q. W., Y.J., Y.S. and J.R.M. performed pharmacological studies. X.W., S.K. and Y-H.L. performed mouse drug treatment and Y-H.L. performed small animal MRI tumor imaging. J.R.M., Y.S., D.K.G., V.C.Y., and F.L.M. generated figures, performed data analysis and statistics. F.L.M. and R.A.D. oversaw the project. V.C.Y. and F.L.M. wrote the manuscript

AUTHOR DISCLOSURES.

Competing Interest Statement.

The authors declare no competing financial interests. F.L.M. and R.A.D. are inventors on a patent covering the concept of targeting ENO1-deleted tumors with inhibitors of ENO2 (US patent 9,452,182 B2). F.L.M., R.A.D., D.M., W.B., Y-H. L., N.S., Z.P., B.C. and F.P. are inventors on a patent application for the use of enolase inhibitors for the treatment of ENO1-deleted tumors (US patent 10,363,261 B2). V.C.Y., C-D.P, and FLM are inventors on a patent application describing the synthesis and utility of novel pro-drug inhibitors of enolase US 62/797,315 (Filed Jan 27, 2019)

R.A.D. is Founder, Director and/or Advisor of Tvardi Therapeutics, Asyilia Therapeutics and Stellanova Therapeutics and the focus of these companies is not related to the content of this manuscript.

Data Availability. There is no restriction in any data presented in this work. The data that support the findings of this study are available from the corresponding author upon request. The POMHEX NCI-60 Human Tumor Cell Lines Screen data are attached as Supplementary Note 2. The Metabolomic data, Figures and Extended Data Figures source data have been deposited in Figshare (doi.org/10.6084/m9.figshare.12931676.v1). The DICOM source MRI scans are stored on a secure sever at MDA and are available upon request.

Accession Codes. X-ray structures of ENO2 bound with HEX(5IDZ) were deposited in PDB.

Code Availability. No custom code or mathematical algorithm used in this study.

⁵Core for Biomolecular Structure and Function, University of Texas MD Anderson Cancer Center, Houston, TX 77054

⁶Institute for Applied Cancer Sciences, University of Texas MD Anderson Cancer Center, Houston, TX 77054

⁷Department of Experimental Therapeutics, University of Texas MD Anderson Cancer Center, Houston, TX 77054

⁸Pharmaceutical Science Facility, University of Texas MD Anderson Cancer Center, Houston, TX 77054

⁹Department of Medicine, Beth Israel Deaconess Medical Center and Harvard Medical School, Boston, MA 02115

¹⁰Director of Drug Discovery and Development, Advanced Organic Synthesis LLC, Houston, Texas, 77054

¹¹Center for Co-Clinical Trials, University of Texas MD Anderson Cancer Center, Houston, TX 77054

¹²Department of Cancer Biology, University of Texas MD Anderson Cancer Center, Houston, TX 77030

Abstract

Inhibiting glycolysis remains an aspirational approach for the treatment of cancer. We previously identified a subset of cancers harboring homozygous deletion of the glycolytic enzyme Enolase (ENO1) with exceptional sensitivity to inhibition of its redundant paralogue, ENO2, through a therapeutic strategy known as collateral lethality. Here, we show that a small molecule Enolase inhibitor, POMHEX, can selectively kill *ENO1*-deleted glioma cells at low nanomolar concentrations and eradicate intracranial orthotopic *ENO1*-deleted tumors in mice at doses well-tolerated in non-human primates. Our data provide *in vivo* proof-of-principal for the power of collateral lethality in precision oncology and demonstrate the utility of POMHEX for glycolysis inhibition with potential across a range of therapeutic settings.

INTRODUCTION.

Glycolysis serves a critical role in cancer metabolism, as elevated glycolytic flux provides essential anabolic support for cellular growth and proliferation. While glycolysis inhibition has been an aspirational target for cancer treatment, the challenge of achieving a sufficiently large therapeutic window for anti-neoplastic activity persists, as it is an essential process performed in all cells. Pharmacologically, this issue is compounded by the sparsity of high-affinity glycolysis inhibitors, with most being tool compounds of limited utility beyond *in vitro* enzymology studies^{1,2}

We previously conceived of and validated an innovative therapeutic strategy known as *collateral lethality*, which capitalizes on cancer-specific metabolic vulnerabilities conferred by passenger deletion of metabolic enzymes neighboring tumor suppressor genes³. One pioneering example of this paradigm includes homozygous deletion of the 1p36 tumor

Owing to the anionic nature of phosphonates, we synthesized a cell-permeable, POM-esterified pro-drug of HEX, POMHEX (Figure 1d; 2, Supplementary Note 1), and compared its selective killing against *ENO1*-deleted glioma cells to the parental free phosphonate. As an esterase-labile pro-drug, hydrolysis of the POM esters would ideally occur by sequential intracellular cleavage by carboxylesterases and phosphodiesterases (Figure 2a). After a one-week treatment course, HEX showed an IC₅₀ of approximately 1.3 μM against D423 cells (*ENO1*^{-/-}), compared to >300 μM against D423 *ENO1*-isogenic rescued and LN319 control cells (*ENO1*-WT; Figure 2b). Treatment with POMHEX gave the same trend at significantly lower concentrations, with an IC₅₀ of approximately ~30 nM against D423 cells, compared to the >1.5 μM against non-target *ENO1*-WT cells (Figure 2d). The pattern of selective sensitivity to POMHEX conferred by *ENO1*-homozygous deletion was confirmed in an independent *ENO1*-homozygous deleted glioma cell line, Gli56^{3,4} (Extended Data Figure 3). To cement the importance of the hydroxamate moiety for chelation to the Mg²⁺ cation, we also tested BenzylPOMHEX, the immediate synthetic precursor to POMHEX (3, Supplementary Note 1). As expected, the absence of a free hydroxamate in the benzyl-protected precursor rendered no selective toxicity against *ENO1*-deleted cells (Supplementary Figure S2), which coincides with our established conclusion that an anionic moiety, such as a hydroxamate, is necessary for active site Enolase inhibition^{4,7,8}.

To support the relationship between *ENO1* deletion status and sensitivity to chemical inhibition of Enolase, we tested HEX and POMHEX against a diverse panel of cell lines as well as through submission to the NCI-60 (POMHEX NCI ID: NSC784584; Supplementary Note 2, Extended Data Figure 4, Supplementary Figure S3) and Sanger Center (POMHEX Drug ID #2148; release scheduled for Q4 2020). On average, POMHEX is about 50-fold more potent than HEX, though with substantial variation across cell lines (Range: 35-fold to 347-fold; Extended Data Figure 4). This range in sensitivity to POMHEX is likely contingent upon both *ENO1* deletion status and varying expression of carboxylesterases and phosphodiesterases. Concurrent with our previous reports with tool compounds^{3,4}, *ENO1*-deleted cell lines were most sensitive to HEX or POMHEX treatment while *ENO1*-heterozygous cell lines displayed intermediate sensitivity (Extended Data Figure 4, Supplementary Figure S3). Some groups of cell lines (e.g. melanomas in NCI-60 dataset and neuroblastomas in the Sanger dataset) were unusually sensitive to Enolase inhibition; however, the sensitivity of *ENO1*-deleted cell lines to Enolase inhibition far surpassed any of these clustered examples. We also independently confirmed the relationship between *ENO1*-deletion status and sensitivity to POMHEX with a series of glioma sphere-forming cells^{9,10} (Extended Data Figure 5). Likewise, amongst the GSCs, GSC296 (*ENO1*^{-/-}) demonstrated greatest sensitivity to POMHEX over a 1-week treatment course. *ENO1*-heterozygous deleted GSCs showed intermediate sensitivity and *ENO1*-WT GSCs were the least sensitive to POMHEX. Interestingly, wild-type lines with low residual expression of ENO2 were more sensitive to POMHEX than those with much higher ENO2 expression (Extended Data Figure 5). To further confirm the on-target effects of POMHEX toxicity and ensure that non-cancerous cells remained unperturbed at the concentrations of POMHEX required to elicit targeted toxicity, we also conducted dose-response experiments on normal and highly differentiated, near-normal cell lines (Extended Data Figure 6). As anticipated, such cells are least sensitive to POMHEX treatment, exhibiting IC₅₀ values comparable or higher than to

those obtained for *ENO1*-WT cancer cells. Thus, our results support the dependence of inhibitor sensitivity on *ENO1*-deletion status. In addition to *ENO1*-deletions, other genetic alterations conferring selective sensitivity are loss-of-function mutations in the von Hippel-Lindau (*VHL*) tumor suppressor gene (which results in a glycolysis-addiction phenotype) and in fumarate hydratase (*FH*), which results in impaired oxidative phosphorylation^{11,12} (Extended Data Figure 7)

Due to the ubiquitous presence of carboxylesterases in biological fluids, degradation of POMHEX to its hemi-ester (HemiPOMHEX) in cell culture media occurs almost entirely within 24 hours. We thus investigated the ability of HemiPOMHEX to retain selective killing of *ENO1*-deleted glioma cells. While we did find that HemiPOMHEX was about 4-fold more potent than HEX, it was significantly less potent than POMHEX against *ENO1*-deleted cells (Figure 2c). This is consistent with previous studies on POM-phosphonates and further supports the greater cell permeability of mono-POM ester phosphonates compared to free phosphonates¹³. Given the instability of POMHEX, we sought to compare the differences between continuous versus pulsed drug treatment. In our pulsed experiments, glioma cells were exposed to POMHEX for 1 hour; thereafter, drug-containing media was replaced by fresh, inhibitor-free media. We found that, while a 1-hour pulse of POMHEX gave nearly identical levels of killing in *ENO1*-deleted glioma cells, these conditions resulted in considerably less killing of the *ENO1*-intact glioma cell lines (Supplementary Figure S4). This suggests that an even wider therapeutic window may be achieved with pulsed, rather than continuous, POMHEX exposure and may be explained by the ability for *ENO1*-WT glioma cells to recover more quickly from Enolase inhibition.

To verify that the observed killing of the target cells was due to on-target glycolysis inhibition by POMHEX, we examined relevant target engagement markers. Inhibitor-treated *ENO1*-deleted cells showed selective depletion of ATP (Figure 2f) and dose-dependent reductions in extracellular acidification rate (ECAR, Figure 2g) in the nanomolar range for POMHEX and in the micromolar range for HEX (Figure 2h). When taking these measurements after short-term exposure to either HEX or POMHEX, we ensured that the number of viable cells was held constant, obviating the possibility that such effects were due to fewer cells (Supplementary Figure S5). Together, these data demonstrate that POMHEX is a potent glycolysis inhibitor, in a manner that is selective for *ENO1*-deleted cells. To provide further evidence that glycolysis inhibition by POMHEX was indeed due to selective inhibition of ENO2, as well as to probe the overall metabolic consequences of glycolysis inhibition, we performed a polar metabolomic profiling.

Metabolic consequences of Enolase inhibition on glycolysis- associated pathways

To further investigate the up- and downstream metabolic consequences of Enolase inhibition, *ENO1*-deleted, *ENO1*-rescued and *ENO1*-intact glioma cells were exposed to increasing doses of POMHEX. Concurrent with our aforementioned findings, such concentrations of POMHEX minimally impacted *ENO1*-WT glioma cells but profoundly affected *ENO1*-deleted cells. Analysis of the effects of POMHEX on protein cell signaling markers (Figure 3a) for cell proliferation (phospho-Histone H3, PLK1), cell death (cleaved caspase-3), and stress (p-NDRG1, p-JunB) revealed 3 salient points. First, even at the

highest concentrations of POMHEX (720 nM), none of these markers were altered in *ENO1*-rescued or *ENO1*-WT glioma cells. Second, in *ENO1*-deleted cells, we observed inhibited proliferation at the lower concentrations of POMHEX (>15 nM, reduction in p-Histone H3) and induction of apoptosis at higher concentrations of POMHEX (>180 nM, increase in cleaved caspase-3). Third, a stress response in *ENO1*-deleted cells becomes evident at ~180 nM of POMHEX (elevated p-NDRG1, p-cJun).

We correlated these cell-signaling markers to metabolite indicators of glycolytic flux (lactate secretion, Figure 3b), Enolase inhibition (glycerate levels, Figure 3c), energy reserves (p-creatine/creatine ratio, Figure 3d), and energy stress (pyrophosphate, Figure 3e). Concentrations of POMHEX that elevate biomarkers of cellular stress, such as p-NDRG1 and p-cJun, concur with metabolite indicators of energy stress, such as a reduced p-creatine/creatine ratios and increased levels of pyrophosphate (PPi). Cell proliferation (p-Histone H3) is inhibited at concentrations of POMHEX (45 nM) that are both too low to induce actual energy stress and only marginally reduce glycolytic flux (Figure 3b). These data suggest that glioma cells have coping mechanisms that link reduced energy production (glycolytic flux) with reduced energy expenditure (proliferation).

To understand the metabolic consequences of inhibiting glycolysis, we performed polar metabolite profiling on the same set of *ENO1*-deleted and *ENO1*-WT cells treated with POMHEX, vide supra. Striking to note was the significant the depletion of metabolites in the citric acid (TCA) cycle (Figure 3f). For instance, we observed a >90% decrease in fumarate despite the supraphysiological concentration of pyruvate in cell culture media (1.25 mM in media versus ~70 μ M in human blood¹⁴). This strongly suggests that, at least in D423 (*ENO1*^{-/-}) cells, glucose catabolism in glycolysis is a major source of anaplerotic substrates for the TCA (Figure 3f), with minor contributions from glutaminolysis or exogenously supplied pyruvate. To verify that exogenous pyruvate was not the main culprit behind toxicity from Enolase inhibition, we repeated the aforementioned POMHEX sensitivity experiments with titrations of pyruvate in cell culture media (Supplementary Figure S6). Omission of pyruvate did sensitize glioma cells to POMHEX, decreasing the IC₅₀ of D423 *ENO1*-deleted cells by about 2.5-fold compared to regular DMEM, which contains 1.25 mM pyruvate (Supplementary Figure S6a **versus** c). Additional supplementation with pyruvate (5 mM) only marginally increased the IC₅₀ (Supplementary Figure S6d). Neither addition of lactate nor acetate meaningfully shifted IC₅₀ (Extended Data Figure 8). Overall, these relatively modest shifts in IC₅₀ values underscore the idea that loss of anaplerotic substrates from inhibiting glucose-derived pyruvate is a minor contributor to the toxicity of Enolase inhibition and that anaplerotic substrates at endogenous physiological levels do not prevent Enolase inhibitor toxicity. Rather, these data suggest that most of the toxicity arises from bioenergetic failure from a loss of glycolytic ATP production (Figures 2f, 3d, and 3e).

While we initially expected that the direct metabolite precursors to the Enolase reaction would experience the greatest alterations in response to POMHEX treatment, we found that the most significant metabolite accumulations occurred at the peripheral arms of glycolysis (Figure 3f). Within the hexose amine biosynthesis pathway (HBP), we observed >15-fold elevations of N-acetyl-glucosamine-phosphate and >60-fold elevations in its hydrolysis product, N-acetyl-glucosamine. Despite these prominent elevations, the pattern of metabolite

alterations in the HBP defies simple interpretation, as we concurrently observed a >90% decrease in the final HBP metabolite, UDP-N-acetyl-glucosamine, in response to POMHEX treatment. We propose that excess metabolic flux from glucose “overflows” into these peripheral carbohydrate metabolic pathways in response to the blocked central flux at the Enolase reaction. These disruptions in the HBP could result in aberrant glycosylation, as HBP metabolites are the main substrates for post-translational protein glycosylation¹⁵. We also observed disruptions in the non-oxidative pentose phosphate shunt¹⁶, with 12-fold elevations in D-sedoheptulose-phosphate (S7P) and erythrose-4-phosphate (E4P; Figure 3f). Both of these metabolites are interconverted with the early glycolysis metabolites, fructose-6-phosphate (F6P) and glyceraldehyde-3-phosphate (GADP), through the action of transaldolases and transketolases. While the functional significance of accumulations in D-sedoheptulose-phosphate and erythrose-4-phosphate remain unclear, such elevations could explain the disruptions in normal flux through the non-oxidative pentose phosphate shunt and the shifted equilibrium of the transaldolase and transketolase reactions which follow. By extension, redox balance and nucleotide pools would be affected, compromising cell viability and likely contributing to the toxicity of Enolase inhibition. We verified that these unexpected metabolite alterations do in fact reflect specific inhibition of Enolase (by POMHEX) through comparison of metabolomic profiles in response to ENO2 knockdown by shRNA (Extended Data Figure 9). Utilizing the same doxycycline inducible shRNA system that we employed previously³, we performed polar metabolomic profiling in response to ENO2 knockdown in D423 *ENO1*-deleted and D423 *ENO1*-rescued cells as a function of time after shRNA induction. The main themes we observed by small molecule Enolase inhibitor treatment (Figure 3) were fully recapitulated by shENO2, in a manner that was selective for *ENO1*-deleted versus *ENO1*-rescued cells (Extended Data Figure 9). Just as with POMHEX, we observed accumulation of metabolites upstream of the Enolase reaction, including overflow into glycolysis-associated pathways and depletion of metabolites downstream of Enolase, such as the TCA cycle.

Antineoplastic activity of POMHEX and HEX against *ENO1*-deleted orthotopic tumors

We conducted safety and toxicity testing for both HEX and POMHEX in nude mice. For administration of HEX, we first neutralized the phosphonic acid with sodium hydroxide. Thereafter, HEX was exceptionally well-tolerated: intravenous (IV) injections at 150 mg/kg per day were tolerated for months without overt signs of toxicity such as hemolytic anemia or loss of body weight. Without neutralization, we found that HEX was only tolerated at IV injections up to 75 mg/kg, which is likely attributed to tissue and blood acidification. We continued our dose escalation toxicity studies, noting the technical challenge of repeatedly performing IV injections at the tail vein of mice. Mice could tolerate IV injections of HEX of up to 300 mg/kg per day with no obvious signs of toxicity. Even in the absence of ill-effects, we note that administering 300 mg/kg of HEX to a 30-gram mouse with a plasma volume of ~2 mL would result in a C_{max} of nearly 20 mM of HEX, which is ~4-fold greater than the concentration of plasma phosphate. Irrespective of effects on Enolase activity, such concentrations of HEX will likely be problematic. To practically achieve higher daily doses of HEX, slow infusion pumps could be used to spread the higher dose over a prolonged period of time. Apart from irritations at the site of injection, subcutaneous injections of HEX were similarly well-tolerated, with no loss of body weight or anemia at 300 mg/kg twice per

day (600 mg/day). At 600 mg/kg twice per day (1200 mg/day), we observed loss of body weight and subcutaneous fat. Both events were reversible upon discontinuation of HEX, testifying to its safety. In contrast, the toxicological profile of POMHEX was quite different. Intravenous injections were consistently tolerated without hemolytic anemia up to 10 mg/kg/day (Supplementary Figure S1), with the maximum single tolerated dose at 30 mg/kg. However, at these higher doses, we observed loss of body weight and subcutaneous fat, which were reversible upon drug discontinuation.

Having established the toxicological profiles of HEX and POMHEX, we then tested their anti-neoplastic effects in intracranial orthotopic *ENOI*-deleted tumors generated from the same D423 glioblastoma cell line used in our *in vitro* experiments. D423 *ENOI*-deleted glioma cells were implanted in the left ventricle area of nude (*Foxn1^{nu/nu}*) mice¹⁷; tumors become T2-MRI detectable around 20–30 days post-implantation. Tumor-bearing mice were then sorted into treatment and control groups see Reporting Summary. Mice were treated daily for 1 week with both IV and intraperitoneal (IP) injection of either HEX (150 mg/kg in PBS) or POMHEX (10 mg/kg in PBS). After 1 week, tumor volumes in the experimental and control arms were measured via T2-MRI. Thereafter, mice were sacrificed for biochemical profiling of pharmacodynamic target engagement markers.

We found that the 1 week treatment resulted in statistically significant attenuated tumor growth compared to non-treated controls (Figure 4a,b). Consistent with our *in vitro* observations, post-mortem analysis of pharmacodynamic engagement markers revealed statistically significant elevations in 3-PG and glycerate compared to non-treated controls (Figure 4c, d). We also performed long-term treatment experiments (>2 weeks) and found complete eradication of *ENOI*-deleted tumors without recurrence after treatment discontinuation (Figure 4m–p). Overall, all tumor-bearing mice in treatment arms across all experiments showed inhibition of tumor growth in response to either HEX or POMHEX (Figure 4a,b,m,n,o,p). For the long-term treatment experiments, complete tumor eradication was observed and complete cures were observed in the 3 out of 5 POMHEX treated mice and in 1 out of 6 HEX treated mice (Figure 4p). The anti-neoplastic effects of Enolase inhibitors against intracranial tumors were independently verified with an independent *ENOI*-deleted glioma cell line, Gli56 (Figure 5). We found that treatment with HEX yields near complete growth suppression (Figure 5a–f), with subsets of tumors showing frank tumor regression (Figure 5f). Even when combined with Avastin, which re-seals the breached blood brain barrier (BBB), HEX was still capable of exerting anti-tumor effects. (Figure 5g). These data show that the anti-neoplastic effects by HEX do not depend on a breached BBB.

We then evaluated the *ex-vivo* pharmacology for POMHEX and HEX (Figure 6, 7). In accordance with the extensive literature on POM pro-drugs^{13,18}, we found that POMHEX is rapidly hydrolyzed to HemiPOMHEX in mouse plasma *ex-vivo*, with a half-life of approximately 30 seconds (Figure 6a). In sharp contrast, the half-life in human blood *ex-vivo* was about 9 minutes. Such pronounced discrepancy in drug metabolism has previously been reported for other POM-containing phosphonate pro-drugs and is attributed to the significantly higher level of carboxylesterase activity in mouse plasma compared to primates and humans^{19–22}. Pharmacokinetic (PK) analysis *in vivo* following single IV or IP injections

of POMHEX in mice concur with the corresponding *ex-vivo* data: intact POMHEX was found to be below quantitative levels in mouse plasma, while both HemiPOMHEX and HEX were readily observed (Figure 6b). In general, much like the esterase-labile pro-drugs of Adefovir and Tenofovir, POMHEX would likely have a more favorable pharmacological profile in humans compared to rodents.

We also performed post-mortem metabolomic analysis on the organs of mice treated with IV/IP injections of POMHEX to characterize the pharmacodynamic profile of POMHEX. Rapid hydrolysis by plasma carboxylesterases resulted in disproportionate accumulation of HEX and greatest degree of Enolase inhibition in the heart (Figure 6c), as indicated by elevations in 3-PG and glycerate (Figure 6d). Given its exceedingly short plasma half-life, the consequently steep concentration gradient away from the site of injection and accumulation in the heart is unsurprising. Both tail vein and IP-injections of POMHEX must traverse through the circulatory system before reaching the tumor (Figure 6c). Thus, only a small fraction of initially injected POMHEX ultimately reaches the tumor. Even in spite of its poor pharmacology, POMHEX is still capable of curing intracranial tumors due to the greater-than-100-fold sensitivity of *ENO1*-deleted glioma cells to Enolase inhibition. It is also possible that anti-neoplastic activity may also be mediated by HemiPOMHEX and HEX—both of which are active against *ENO1*-deleted cells in culture (Figure 2b–d), with the latter being active against *ENO1*-deleted intracranial tumors, though at higher doses than POMHEX (Figure 4,5).

The absence of any carboxylesterase-labile moieties on HEX rendered a much more favorable pharmacodynamic profile when administered at doses 15 times higher than POMHEX. Lactate levels were not significantly decreased in any organ or in plasma and glycerate accumulations were found exclusively in the brain (Figure 6d). Notably, *ENO1*-deleted brain tumors showed a similar degree of elevation in 3-PG and glycerate for (higher-dosed) HEX as for POMHEX (Figure 6d). These data are particularly striking, as HEX is a highly polar, anionic molecule that is unlikely to permeate an intact BBB. While breached BBBs are characteristic of GBM²³, our experiments examining the effects of Avastin on HEX treatment strongly suggest that HEX does not permeate intracranial tumors through a breached BBB (Figure 5). Avastin is an anti-angiogenesis monoclonal antibody that seals and thus decreases the permeability of the BBB²⁴ (Figure 5).

HEX most likely reaches the brain and brain tumor by permeating the blood/cerebrospinal fluid barrier, which is known to allow small, highly polar drugs, such as Fosfomycin, to pass through fenestration in the endothelial cell layer²⁵. Fosfomycin, a close structural analogue to HEX, is present at a 1:10 plasma to cerebrospinal fluid barrier ratio^{26,27}. As HEX induces brain-specific elevations in pharmacodynamic markers of Enolase inhibition (Figure 6d) strongly suggests that it indeed permeates the brain to exert its anti-neoplastic activity. These data suggest that greater on-target, selective inhibition of Enolase in the brain can be achieved with HEX, compared to POMHEX.

High exposure and favorable safety profile of Enolase inhibitors in primates

Having established the safety and efficacy profiles of both HEX and POMHEX in murine models, we then tested their toxicity and PK profiles in the non-human primate model

(NHP) *Cynomolgus*. (Figure 6, 7, Extended Data Figure 10, Supplementary Figure S7 and S8). Compared to our experiments in mice, we worried that POMHEX might exhibit greater potency and toxicity in primates, as the lower carboxylesterase activity and metabolic rate in the latter could result in longer drug half-life and higher drug exposure. We thus began our primate studies using a single dose of POMHEX at 2.5 mg/kg (n=3). Similar to our findings in mice, no intact POMHEX could be detected (minimum limit of ~100 nM) even at the earliest timepoint after injection. However, we found that both HemiPOMHEX and HEX had 10-times longer half-lives and thus, higher drug exposure, in primates compared to mice (Figure 6b), which is typical for phosphate and phosphonate drugs^{28–30}. We then escalated the IV dose of POMHEX to 10 mg/kg, noting the absence of any significant anemia, weight loss, or other adverse effects. Excluding values attributable to post-collection hemolysis, blood chemistry values were normal. Escalating to 20 mg/kg was also well-tolerated (Supplementary Figure S7). However, IV injection of 35 mg/kg of POMHEX resulted in lethargy that prompted veterinarians to perform euthanasia. Notably, even at this high dose, no hemolysis or anemia was evident (Supplementary Figure S7). We suspect that long-term (>19 hours) pre-dose fasting lowered blood glucose levels in the cynomolgus monkey; treatment with POMHEX may have led to hypoglycemia from Enolase inhibition in gluconeogenic tissues such as the kidney and liver. As we did not expect this hypoglycemic lethargy at 35 mg/kg of POMHEX, no contingency measures were established in the protocol. Had we anticipated this outcome, a simple glucose infusion would have been sufficient to resolve this issue. A similar pattern of generally favorable tolerability was also observed for HEX. Subcutaneous injections at 100 mg/kg and 200 mg/kg were well-tolerated without adverse events (Figure 7a–d) despite plasma exposures vastly higher than mice, sustaining levels far higher than those required for efficacy even against *ENO1*-heterozygous deleted cells (Figure 7a). Dosing at 400 mg/kg resulted in lethargy with severe hypoglycemia (Figure 7b–d); veterinarians performed euthanasia as contingency measures were not established in the protocol, again, presumably due to the inhibition of gluconeogenesis. We performed repeated S.C. injection of HEX at 100 mg/kg QD and 120 mg/kg BID for 4 days and 10 days respectively. Both treatment courses were tolerated without adverse events. Ultimately, these experiments demonstrate that therapeutically efficacious doses of POMHEX or HEX are well-tolerated in primates. The lower activity of carboxylesterases in primates enables longer drug exposure and perhaps decreased organismal sensitivity to POMHEX due to slower pro-drug activation. The highly favorable safety profile for both POMHEX and HEX coupled with longer drug exposure in primate plasma strongly suggest that anti-neoplastic therapeutic efficacy can be easily achieved in primates and, by extension, in the clinic.

DISCUSSION.

We have described an ENO2-preferential Enolase inhibitor that selectively kills *ENO1*-deleted glioma cells in culture and exhibits robust anti-neoplastic activity against *ENO1*-deleted xenografted orthotopic intracranial tumors in murine models. Due to the anionic nature of the phosphonate moiety on HEX, we generated POMHEX, a POM-esterified pro-drug that exhibits nanomolar potency in cell culture and is capable of eradicating *ENO1*-deleted intracranial orthotopic tumors in mice at 15-fold lower than that administered for the

non-pro-drug HEX. Indeed, POMHEX proved to be dramatically more effective than HEX at inducing tumor regression on a per-molar basis (Figure 4). Nonetheless, HEX was quite effective at inhibiting Enolase and tumor growth in the brain, despite its poor permeability. Clinical effects of phosphonate drugs in brain pathologies have been reported even in the absence of an obvious breach of the BBB^{31–39}. The literature is also laden with examples of evidencing the ability of low molecular weight phosphonates to permeate the blood-cerebrospinal fluid (CSF) barrier^{31–35}. Our findings with HEX strongly suggest that, much like its structural relatives Fosfomycin²⁵ and Fosfarnet⁵², HEX likely permeates the blood-CSF barrier to exert its anti-neoplastic activity.

Though POMHEX is clearly capable of demonstrating anti-neoplastic activity, our *in vivo* and *ex vivo* pharmacokinetic studies evidence the instability of the POM pro-drug group by the steep concentration gradient of intact drug away from the site of injection (Figure 6c). Greater elevations in 3-PG and glycerate in visceral organs compared to the brain suggest that little intact POMHEX reaches the brain. On its own, there is no obvious reason that precludes POMHEX from crossing the BBB, with its predicted logP of 0.76, single hydrogen bond donor, and sufficiently low molecular weight⁵³. Given the robust anti-tumor activity we observe with POMHEX, it is quite possible that such effects may be attributed to the combined penetration of HemiPOMHEX and HEX through the blood-CSF barrier. Indeed, the challenge of extrapolating the metabolism of carboxylesterase-labile substrates in rodents to primates lies in the 80-fold higher carboxylesterase activity in the former^{19–21}. While the instability of intact POMHEX was consistent in both murine and primate models, our PK studies in the latter evidenced the prolonged half-life and drug exposure of HemiPOMHEX compared to that observed in mice. Most importantly, our PK experiments in primates showed that POMHEX was fully tolerated at and above the doses required for therapeutic efficacy in murine models of GBM while achieving much higher drug exposures. Thus, in spite of the sub-optimal pharmacology of intact POMHEX, our pre-clinical data strongly suggest that Enolase inhibition would be effective against *ENO1*-deleted tumors in patients. The lability of the POM group is not ideal for delivering HEX. Pro-drug moieties with alternate mechanisms of bioactivation have been synthesized¹³ and is an ongoing area of research in our laboratory. One promising pro-drug strategy capitalizes on elevated expression of nitroreductases under hypoxic conditions^{54,55}, a defining characteristic of many tumors such as GBM⁵⁶. Such application to HEX could result in a more favorable distribution of Enolase inhibition in tumor versus surrounding tissues. Future work will be directed towards evaluating this strategy and other bioactivation strategies as alternative pro-drug approaches^{55,57,58}.

While the focus of this paper is on GBM, homozygous deletion of *ENO1* at the 1p36 locus also occurs in hepatocellular carcinoma, cholangiocarcinoma and large cell neuroendocrine lung tumors³; all poor-prognosis cancers with limited treatment options. Though we have extensively discussed the rationale of Enolase inhibition in the context of *ENO1*-homozygous deleted cancers, our data also allude to the intermediate sensitivity of *ENO1*-heterozygous deleted cancer cells (Supplementary Figure S3, Extended Data Figure 4), which can expand the application of collateral lethality in the clinic. PK experiments indicate that drug exposures required for efficacy against *ENO1*-heterozygous deleted cancer cells can be sustained in NHP even though not in mice (Figure 7a). Our data also show

selective sensitivity in mitochondrial oxidative phosphorylation deficient cancers driven by TCA cycle loss-of-function mutations as well as those “addicted” to glycolysis due to mutations in VHL^{11,12,59} (Extended Data Figure 7). Beyond these defined genomic populations with Enolase deficiencies, unique sensitivity to Enolase inhibition has also been documented in other genetic settings^{60,61} testifying to greater utility of POMHEX and HEX. Thus, for the first time, we have provided *in vivo* proof-of-principle for the decisive efficacy of collateral lethality through pharmacological inhibition of Enolase. Our data cement the viability of translating our approach to the clinic and, amidst the extensive catalogue of passenger-deleted metabolic genes in cancer, support the capability of collateral lethality to significantly expand the scope of actionable genetic alterations for precision oncology.

Finally, the Enolase inhibitors described herein are useful tools for further probing the role of glycolysis intermediates in metabolic pathologies beyond cancer. Investigations into glycolysis have historically relied on 2-deoxyglucose, an early upstream inhibitor of glycolysis. HEX and POMHEX intervene late in glycolysis, presenting opportunities to investigate the roles of later glycolysis metabolites in glucose sensing for beta cells⁶² or post-translational histone lactylation⁶³.

METHODS.

Chemical synthesis and quality control.

Initial syntheses of HEX and POMHEX were performed at M.D. Anderson’s Pharmaceutical Chemistry Facility. Subsequent syntheses were contracted to WuXi Apptec, Shanghai, China. Full synthetic descriptions are provided in Supplementary Note 1. Product integrity was verified in-house by ¹H, ³¹P, ¹³C NMR and UPLC-MS.

Enolase enzymatic activity assay and inhibitor titrations.

Enolase activity was measured *in vitro* using a plate reader as previously described^{3,4,64}. For Michaelis-Menten titrations, Enolase substrate concentrations were titrated from 10 mM in 2-fold dilutions.

Enolase inhibitor toxicity testing *in vitro* and cell lines.

Cell culture experiments to test Enolase inhibitor sensitivity were conducted in 96-well plates. Plates were seeded at around 15% confluence. Cancer cells were attached for 24 hours and were treated with fresh media containing Enolase inhibitor. Columns 1–2 and 11–12 were used as vehicle media only CTs. Columns 3–10 were used for drug treatment in 2-fold concentration gradients. After 6–7 days of growth, plates were washed with phosphate buffered saline (PBS) and fixed with 10% formalin. Fixed plates were stained with 0.1% crystal violet^{65,66} and quantified by acetic acid extraction with spectrophotometric absorption at 595 nm in a plate reader. Cell densities were expressed relative to non-drug, media-only wells. Unless stated otherwise, all experiments were conducted in DMEM media with 4.5 g/L glucose, 110 mg/L pyruvate and 584 mg/L glutamine (Cellgro/Corning #10-013-CV) with 10% fetal bovine serum (Gibco/Life Technologies #16140-071) and 1% Pen Strep (Gibco/Life Technologies#15140-122) and 0.1% Amphotericin B (Gibco/Life Technologies#15290-018).

The main cell line used in this work is the H423/D423-MG (CVCL_1160, Glioblastoma), a 1p36 homozygous deleted cell line that is referred to as D423 throughout the manuscript. Details about the origin and genes deleted in the D423 cell line were given in our previous work⁴ as well as the *ENO1*-WT cell line LN319, a sub-clone of LN-992⁶⁷ (CVCL_3958, Glioblastoma). The isogenic control cell line, D423 *ENO1*, where ENO1 is re-expressed ectopically, and the *ENO1*-heterozygous deleted glioma lines D-502MG (also known as H502⁶⁸, CVCL_1162, Glioblastoma) and U343-MG⁶⁹ (CVCL_S471, Glioblastoma) were described previously³. The Gli56 cell line is a 1p36/*ENO1* homozygously deleted glioma cell line described previously⁴ and the two isogenic Gli56 ENO1 rescued cell lines one with ENO1 alone, and a second with rescue of both ENO1 and NMNAT1 as described previously³. All other cell lines (NB1(CVCL_1440, Neuroblastoma), U87(CVCL_0022, Glioblastoma), A1207 (CVCL_8481, Glioblastoma), HepG2 C3A (CVCL_1098, Hepatoblastoma), HEK293 (CVCL_0045), SNU423, (CVCL_0366, Adult hepatocellular carcinoma), SNU398 (CVCL_0077, Adult hepatocellular carcinoma), SK-HEP-1 (CVCL_0525, Adult hepatocellular carcinoma)) were from the MD Anderson Genomic Medicine Cell line Core. Astrocytes are from ScienCell Research Laboratories (1800). The cell lines were authenticated at the MD Anderson Cytogenetics and Cell Authentication Core.

Western blots.

Cell lysates were washed in ice cold phosphate-buffered saline (PBS). They were then collected in cold RIPA buffer with protease (Complete mini, Roche) and phosphatase inhibitors (PhosSTOP, Roche), and then sonicated. Protein concentration was determined by BCA assay (ThermoFisher 23227), separated by SDS-PAGE (4–12% gradient), and transferred onto PVDF membranes using the Semi-Dry method (TransBlot turbo). Membranes were verified for efficient transfer with Ponceau S staining. Membranes were then blocked with 5% non-fat dry milk in TBS with 0.1% Tween 20 (TBST). Primary antibodies were incubated overnight at 4°C with gentle rocking. They were then washed 4x for 5 min with TBST. This was followed by secondary antibody incubation at room temperature for 1 hour with gentle rocking. Then, the membranes washed 4x for 5 min with TBST and incubated with ECL (ECL prime GE Healthcare (RPN2236)) or (ThermoScientific SuperSignal West Femto (34096)). Films were exposed in a dark room and developed following standard procedures. Antibodies used were at 1:1000 dilution in Blocking buffer; Cleaved Caspase-3 (CST#9664), PLK1 (CST#4513), phospho-Histone H3 (S10) (Epitomics 1173–1), phospho-NDRG1 (T346) (CST#5482), phospho-C-Jun (S73) (CST#3270), and 1:5000 dilution of Vinculin (CST#13901). ENO2 (Dako M087301-2 1:5000, Lot : 20017543); ENO1 (Abcam ab155102; 1:10,000, Lot: GR257281-15); GAPDH (SIGMA G9545 Lot: 127M4814V); TPI1 (ProteinTech; 10713-1-AP 1:5000, Lot 1). Secondary Antibodies were used at 1:5000 dilution, Anti-rabbit IgG HRP-linked Antibody (CST#7074).

Experimental animals.

All experiments involving mice performed at the UT MD Anderson Cancer Center were approved by MD Anderson's Institutional Animal Care and Use Committee (IACUC). Swiss nude or NSG-NOD scid female mice, 3–6 months old, were used. Mice were obtained

from the Experimental Radiation Oncology at UT MDAnderson Cancer Center or the Jackson Laboratory and were housed in 12-hour light/12-hour dark cycle, in temperature (68–72°F) controlled and humidity (30–70%) monitored rooms. Controls mice are from the same cage as the treated mice but since they were purchased, may or may not be genetically related (littermates). All non-human primate experiments were performed by Charles River Laboratories as a fee-for-service. All procedures were approved by Charles River's IACUC committee. Male, adult cynomolgus monkeys (*Macaca fascicularis*), also known as crab eating macaque, weighing between 2.5–3.5 kg were used. All animals were under continuous veterinary supervision. All animals assigned to the study were acclimated (restrain, dose administration, blood collection, etc.) within 2 weeks prior to dosing. All technicians who perform relevant procedures were trained and signed off. In addition to twice-daily health checks by the animal care staff, animals will be observed for any clinically relevant abnormalities during dosing and at each sample collection. Animals with clinical signs deemed by the Test Facility Veterinarian to cause pain or distress would be euthanized or appropriate veterinary care administered based on veterinary recommendations and in consultation with the study director. Euthanasia follows Charles River IACUC approved protocol of overdose by Ketamine + Euthasol. After completion of the study, animals were returned to the main colony.

Retro-orbital bleeding and hematocrit determination.

Mice were anesthetized using isoflurane. Blood was collected using heparinized microhematocrit capillary tubes (Fisherbrand #22-362574) through retro-orbital and was sealed with hemato-seal capillary tube sealant (Fisherbrand #02-678). First, slight pressure was applied on the eyeball to stop the bleeding. Then, Proparcanie was applied on the eye to decrease the pain after the procedure. The capillary tubes were spun at 1,500xg for 10 minutes. The hematocrit was calculated by dividing the measured height of red blood cell layer by the total height of the blood.

Intracranial orthotopic tumor cell implantation.

Intracranial glioma cell injections were performed by the M.D. Anderson Intracranial Injection Core at M.D. Anderson (Dr. Fred Lang, Director⁷⁰). Intracranial tumors were established by injection of 200,000 cells into the brains of immunocompromised female nude *Foxn1^{nu/nu}* mice ages 4–6 months, which were bred at the Experimental Radiation Oncology Breeding Core in M.D. Anderson. The animals were first bolted (a bolt is a plastic screw with a hole in the middle which is driven into the skull⁷⁰) and allowed to recover for 2 weeks. Then, glioma cells were injected through the bolt with a Hamilton syringe. Bolting and cell injections were performed by the M.D. Anderson Intracranial Injection Fee-for-Service Core⁷⁰. The animals were euthanized when neurological symptoms became apparent.

Small animal MRI and tumor volume calculation.

MRI was performed in a 7T Biospec USR707/30 instrument (Bruker Biospin MRI, Billerica, MA) at the M.D. Anderson Small Animal Imaging Facility (SAIF), located in the same building as our mouse colony. Animals can thus be imaged serially with minimal difficulty. First, the animals are briefly maintained under deep anesthesia using Isoflurane. Body

temperature was maintained with a heating blanket. Anesthetized mice were restrained using a stereotactic holder to hold their heads. Breathing was monitored and synchronized with the instrument. Routine tumor detection was done by T2-weighted imaging. First, a low-resolution axial scan is taken to properly center the field. Then, a series of high-resolution axial and coronal scans are recorded. The RadiAnt DICOM Viewer software was used for the image analysis.

For tumor volume calculations, we use the “ellipse” command from the tool bar to circle the tumor area in each tumor slides. The software converts the selected area from pixels to cm^2 . The axial or coronal tumor volume was calculated as both the sum of tumor volumes in each slide and the estimated tumor volume of the space in-between slides. Tumor volume for slides were calculated as the area from the RadiAnt. For coronal slicing, a thickness of 0.75 mm was used. For axial slicing, a thickness of 0.5 mm was used. For tumor volume estimations of the in-between slides, the average tumor area between the two slices was multiplied by the distance between the two slices (0.25mm for coronal slicing and 0.5mm for axial slicing). Tumor volume was then calculated as the average of coronal and axial tumor volumes.

Polar metabolite profiling.

Culture media was removed from the plate and saved for lactate secretion determination. Adherent cells were washed once with cold PBS and aspirated completely. Four μL of ice cold 80% methanol were added to each 10 cm round plate. Plates were stored at -80°C for 20 min. Cells were scraped from the plates on dry ice and transferred with the methanol to a pre-cooled 15mL conical tube. Next, the tube was vortexed for 5 sec and spun down at $14,000\times g$ for 5 min at $4-8^\circ\text{C}$ to pellet the cell debris. The metabolite-containing supernatant was transferred to a clean pre-cooled 15-mL conical tube. This was then aliquoted in 1 mL fractions in 1.5 mL Eppendorf tubes and dried in the SpeedVac. The dried metabolite samples were run by tandem mass spectrometry (LC-MS/MS) via selected reaction monitoring (SRM) with polarity switching for 300 total polar metabolite targets using a 5500 QTRAP hybrid triple quadrupole mass spectrometer (SCIEX). MS was coupled to a HPLC (Shimadzu) with an amide HILIC column (Waters) run at $\text{pH}=9.0$ at $400\ \mu\text{L}/\text{min}$. Q3 peak areas were integrated using MultiQuant 2.1 software⁷¹.

Xenografted mouse drug treatment with POMHEX and HEX.

POMHEX was dissolved in DMSO at 200 mM and stored at -80°C . Aliquots of POMHEX DMSO stock were dissolved in PBS to achieve the desired quantity (typically 10 mg/kg, if not otherwise indicated). The total volume of $200\ \mu\text{L}$ PBS ($<2\%$ DMSO) was injected intravenously or intraperitoneally. HEX was dissolved in water to a concentration of 1M. For administration of HEX, we first neutralized the phosphonic acid with sodium hydroxide to generate the monosodium salt. The mouse was restrained with the Tailveiner Restrainer (Braintree Scientific #TV-150 STD). For intravenous injections, the tail was soaked in warm water for 1 min to stimulate the vasodilation, A 30G insulin syringe (BD #328431) was used for injection through lateral veins.

Seahorse glycolytic flux (ECAR) and respiratory capacity (OCAR) determinations:

The glycolytic capacity of D423 and D423 ENO1 rescued cell lines exposed to POMHEX was assessed using XF Glycolysis Stress Test Kit (Seahorse Bioscience) according to the manufacturer protocol. Briefly, 40×10^4 cells/well were plated on a 96-well Seahorse microplate 24 hours before the experiment. (DMEM supplemented with 10% FBS and 1% Pen-Strep). The medium was replaced 1 hour before the experiment with Glycolysis Stress Test Assay Medium supplemented with 2 mM L-glutamine. Cells were then incubated at 37°C (low CO₂) for 1 hour. The Seahorse cartridge was hydrated for 24 hours in calibrating solution (Seahorse Bioscience) followed by loading with POMHEX - PORT A (concentration range from 1 μM to 0.062 μM), glucose (10 mM) - PORT B and oligomycin (2.5 μM) - PORT C. The extracellular acidification rate (ECAR) was measured using the Seahorse XF analyzer (Seahorse Bioscience). POMHEX was added for 150 minutes before glycolytic capacity of the cells was assessed. After measurement, the cells were fixed for 10 minutes in 10% NBF followed by 15 minutes incubation in Hoechst 33332. The fluorescence of each well was quantified using Tecan Infinite M200PRO Plate Reader.

Pharmacokinetic quantification of POMHEX and its metabolites.

POMHEX: 25 μL of plasma sample, including the analytical standards and quality controls (QCs), were mixed with 200 μL of Acetonitrile. After vortex and centrifugation, 100 μL of the supernatant was mixed with 100 μL of water for LC-MS/MS analysis. The same procedure was followed for the preparation of cell lysate samples.

HemiPOMHEX and HEX: 50 μL of plasma sample including the standards and QCs were diluted with 500 μL of 10 mM aqueous NH₄HCO₃ containing Bn-HEX (0.015 μM, internal standard). This was then loaded onto a Waters Oasis MAX SPE cartridge (30 mg) which was pre-conditioned with methanol (1 mL) and water (1 mL). The cartridge was washed with water (1 mL) and methanol (1 mL). Analytes were derivatized on the cartridge with 200 μL of 2.0 M solution of trimethylsilyl-diazomethane in hexane (TMS-DAM, Sigma Aldrich) for 1 hour to obtain TMS-derivatized Hemi-POM-HEX and HEX. The derivatized analytes in the cartridge were eluted with methanol (1 mL), evaporated to dryness at 40°C under a stream of nitrogen, and reconstituted with 150 μL of 0.1% FA in water/ ACN (2:1) for LC-MS/MS analysis. The same procedure was followed for the preparation of cell lysate samples. Samples were analyzed on an Agilent 1290 Infinity Binary LC/HTC Injector coupled to a Sciex 5500 Triple Quadrupole Mass Spectrometer operated in positive mode. The mass spec source conditions were set for all the analytes as the following: ion spray voltage (5500 volts), curtain gas (35), collision gas (8), gas temperature (500°C), ion source gas 1 (40), ion source gas 2 (60), DP (156), EP (10), CE (27), CXP (10). The LC mobile phase A was 0.1% acetic acid-water and B was 0.1% acetic acid-acetonitrile. The LC flow rate was 0.5 mL/min. The injection volume was 2 μL. The column temperature was set to 40°C. POMHEX was separated using a Supelco Ascentis fused-core C18 (2.7 μm, 2.1 × 20 mm) column (Sigma-Aldrich, St. Louis, MO) and detected by a multiple reaction monitoring transition (m/z 424.1>280.1). The LC gradient was 25% B (0–0.3 minutes), 25–95% B (0.3–1.3 minutes), 95% B (1.3–1.7 minutes), 95–22% (1.7–1.71 min), 22% B (1.71–2.0 min). Under these conditions, the retention time of POMHEX was 1.08 minutes. The method was validated with an analytical range of 5 – 1000 ng/ml for POMHEX in untreated CD-1 mouse

plasma. The acquired data was analyzed using Sciex MutiQuan 3.0.2 software. The TMS-derivatized HemiPOMHEX and HEX were separated using a Phenomenex Luna C8 (3 μm , 2.0 \times 50 mm) column (Torrance, CA). The multiple reaction monitoring transition was 360.4>330.1 (TMS-HemiPOMHEX), 238.1>207.0 (TMS-HEX), and 313.9>91.1 (TMS-Bn-HEX, IS). The LC gradient was 5% B (0–0.3 minutes), 5–95% B (0.3–1.5 minutes), 95% B (1.5–2 minutes), 95–22% (2–2.1 minutes), 22% B (2.1–2.3 minutes). Under these conditions, the retention times were 0.97 minutes (TMS-HEX), 1.30 min (TMS-Hemi-POM-HEX), and 1.26 min (TMS-Bn-HEX, IS). The method was validated with an analytical range of 0.1 – 5 μM for both Hemi-POMHEX and HEX in untreated CD-1 mouse plasma.

Quantification of HEX, glucose and lactate in plasma by NMR.

Due to the toxicity of the derivatization procedure to measure HEX by mass spec, we devised an alternative quantification method using NMR. Two hundred μL of plasma was extracted with 2 volumes of dry ice-cold methanol incubated at $-20\text{ }^{\circ}\text{C}$ for 45 min, and the protein precipitate was separated by centrifugation (17,000 $\times g$ for 30 minutes at $4\text{ }^{\circ}\text{C}$). We then concentrated the supernatant by speedVac for 4 hours and resuspended in 470 μL D_2O (Sigma Aldrich, 151882) and 30 μL D_2O with 3% TPS as an internal standard (Sigma Aldrich, 450510). We utilized a Bruker Avance III HD 500 MHz NMR spectrometer equipped with broadband observe cryoprobe. For each sample, we acquired 1D ^1H spectrum (zg30 pulse program), 1D ^1H spectra with inverse gated ^{31}P decoupling (zgig pulse program) and 2D ^1H - ^{31}P HSQC (hsqcetgp pulse program, gpz2 %=32.40, ^{31}P spectral width= 40 ppm, O2p=0 ppm, cnst2=22.95 and 128 scans). We used ^1H spectra to calculate concentration of lactate and glucose with reference to the TSP peak. To quantify HEX concentration in plasma, we utilized a 2D ^1H - ^{31}P heteronuclear single quantum correlation (HSQC) technique which benefits from higher sensitivity compared to 1D ^{31}P NMR. Signal form ^1H - ^{31}P HSQC were projected in the ^{31}P dimension using the “proj” commend in TopSpin. The 15 ppm peak in the ^{31}P spectrum appeared exclusively in HEX-treated samples. No peaks above 6 ppm were ever observed in non-treated plasma which is consistent with the absence of phosphonates (only phosphates) in biological samples. Quantification was performed by integrals, with ^1H spectra and TSP used as reference to calculate molarity.

PK and PD studies in non-human primates.

Animals were fasted overnight, with food returned 4 hours post injection (~12–17 hours fasting time in total). POMHEX was dissolved in DMSO at 100 mg/ml and prepared for injections by dilution with normal saline to desired concentration and filtration. POMHEX was administered at nominal doses of 2.5, 10, 20 and 35 mg/Kg as an IV bolus dose. HEX was dissolved in water at 150 mg/mL with pH adjusted to 7.2–7.4, and further diluted with saline to desired concentration and filtered using 0.22 μm filter before administration. HEX was administered as a subcutaneous injection at 100, 200 and 400 mg/Kg. BenzyHex was handled and injected same as HEX. Blood samples were collected pre-dose and post dose, over 24 hours, for PK- hematology analysis (K_2EDTA was used as anticoagulant and PMSF (Sigma # 10837091001) as an esterase inhibitor in the collection tubes of the POMHEX study) and clinical chemistry (serum) analysis. Blood glucose, lactate as well as Blood chemistry and hematology vet panels were carried out at Charles River Laboratories. The

primates' health was monitored for 1 week in the lab for any adverse event after return to the main colony.

Lactate secretion determinations by NMR.

Cell culture media was spun down at 14,000 g for 10 minutes at 4°C. The supernatant was transferred to a clean, pre-cooled 50 mL conical tube. Then, 40 mL of pre-cooled methanol was added to the 10 mL of supernatant to make a final 80% (vol/vol) methanol solution. The mix was gently shaken and incubated overnight at -80°C. Next the mixture was spun down at 14,000 g for 10 minutes (4-8 °C). The supernatant was transferred to a new 50 mL conical tube and dried in the SpeedVac. The dried metabolites were re-suspended with 400uL of D2O and 50uL of D2O with TMS (ALDRICH #450510) for NMR analysis. A 500 MHz Bruker Avance III HD NMR equipped with a Prodigy BBO cryoprobe instrument was used. Conditioned media was supplemented with 10% D2O for signal lock and 3-(trimethylsilyl)propionic-2,2,3,3-d4 acid standard. Lactate exhibits a highly characteristic, strong doublet peak at 1.4 ppm in the 1H spectrum, which was quantified by integration relative to the 3-(trimethylsilyl)propionic-2,2,3,3-d4 acid standard at 0 ppm.

ENO2:HEX crystal structure:

Apo crystals of Human Enolase 2 were prepared using the hanging drop vapor diffusion method at 20°C, suspending a drop containing 0.5 µL 9.1 mg mL⁻¹ Enolase 2 and 0.5 µL reservoir solution above a 500 µL reservoir containing 200 mM ammonium acetate, 100 mM Bis-Tris and 18–22% (w/v) PEG 3350. Streak seeding in the same solution conditions reproducibly produced larger crystals. The crystals were soaked overnight in 1 µL drops containing 100 mM Bis-Tis, 200 mM ammonium acetate, 32% (w/v) PEG 3350 at pH 6.5, supplemented with 2 mM HEX compound, prior to flash freezing in liquid nitrogen. An X-ray diffraction dataset was collected at 100 K using the Advanced Light Source Beamline 8.3.1 equipped with ADSC Q315r detector. 360 images with 1° oscillation were collected, using 1.116 Å wavelength. The diffraction images were indexed and integrated using iMOSFLM⁷² and scaled using AIMLESS⁷³. The X-ray structure was solved by molecular replacement with a human Enolase 2 homodimer (PDB code 4ZCW) as the search model. The structure was iteratively refined using Coot⁷⁴ and phenix.refine^{75,76}.

Immunohistochemistry for Markers of Proliferation and Cell Death

Tumor bearing mice were sacrificed and immediately placed in 4% phosphate buffered formalin. Brains with xenografted tumors *in situ* were dissected and sent for dehydration, paraffin embedding and tissue sectioning was performed by M.D. Anderson's Veterinary Pathology Core. Slides were left to incubate at 60°C overnight, de-paraffinated with xylene and re-hydrated with a gradients of ethanol water mixtures. After re-hydrations, slides were subjected antigen retrieval in citrate buffer [1:100 Vector Antigen Unmasking Solution (Citrate-Based) H-3300 250 mL] for 10 minutes at boiling temperature, followed by 30 minutes cooling. Sections were covered with a blocking buffer of 2% goat serum [Vector S-1000 Normal Goat Serum 20 mL] in PBS [Quality Biological PBS (10X), pH 7.4 1000 mL] for 1 hour. Sections were then covered with anti-Cleaved Caspase 3 rabbit monoclonal (Cleaved Caspase-3 (Asp175) (5A1E) Rabbit mAb; CST# 9664T, Cell Signaling Technology) in a 1:1000 dilution or anti-phospho S10 Histone H3 (Rabbit anti-Phospho Histone H3 (S10)

IHC Antibody, Affinity Purified; Bethyl Laboratories, IHC-00061) with 2% goat serum in PBS and left to incubate overnight in 4°C. Sections were then washed in PBS and incubated for 30 minutes with [Invitrogen by Thermo Scientific 1X goat anti-rabbit IgG secondary antibody, poly HRP conjugate]. After washing in PBS and Tween 20 [Fisher BioReagents BP337-500], Sections were developed using either ImpactNOVared (Vector Labs; yields a red-to brown color for stain) or using EnzMet™ (Nanoprobes #6001-30 mL; yields a black stain). For NOVared, slides were then counterstained using hematoxylin; for EnzyMet, slides were counterstained with hematoxylin and optionally, eosin counterstain. Sections were mounted using Denville Ultra Microscope Cover Glass (Cat# M1100-02) and Thermo Scientific Cytoseal 60 and left to dry overnight.

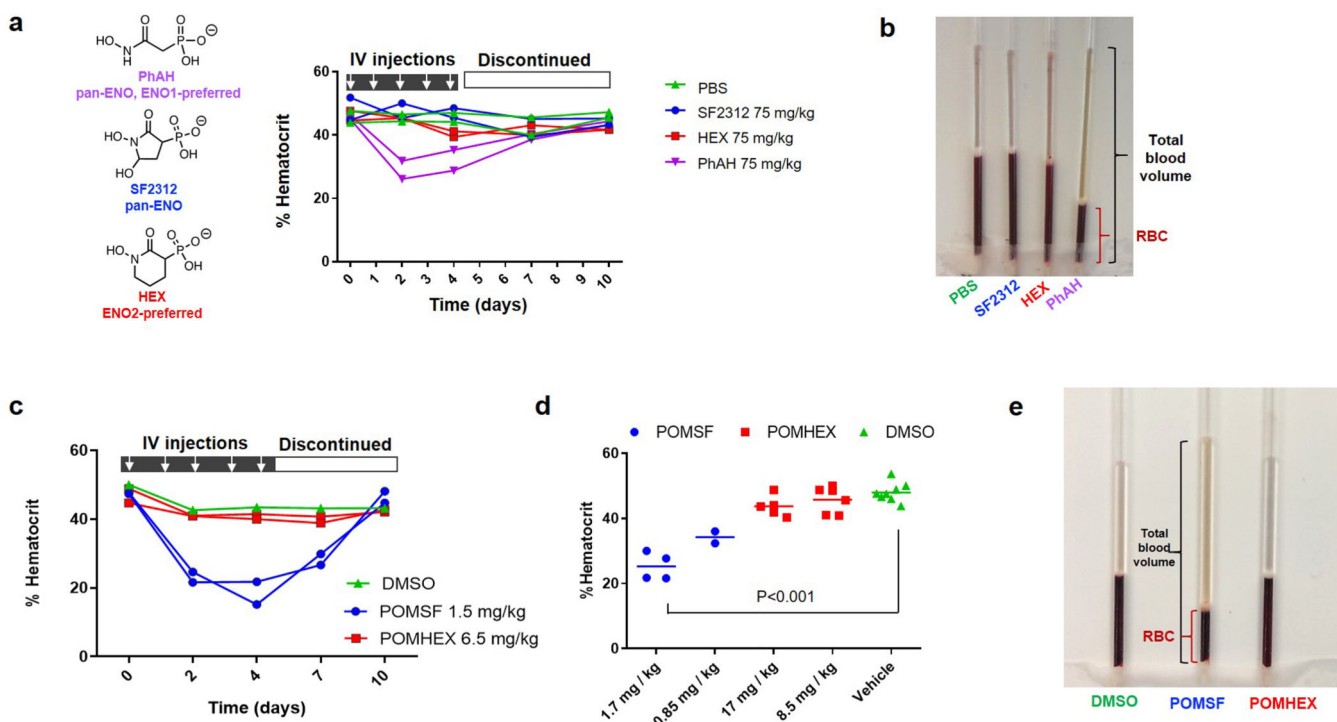
Half-life comparison between HEX and other phosphonate-containing drugs.

Values used in the systematic comparison between the plasma half-lives of other phosphonate-containing drugs and HEX were obtained from the literature⁴⁰⁻⁵¹.

Statistical Analysis.

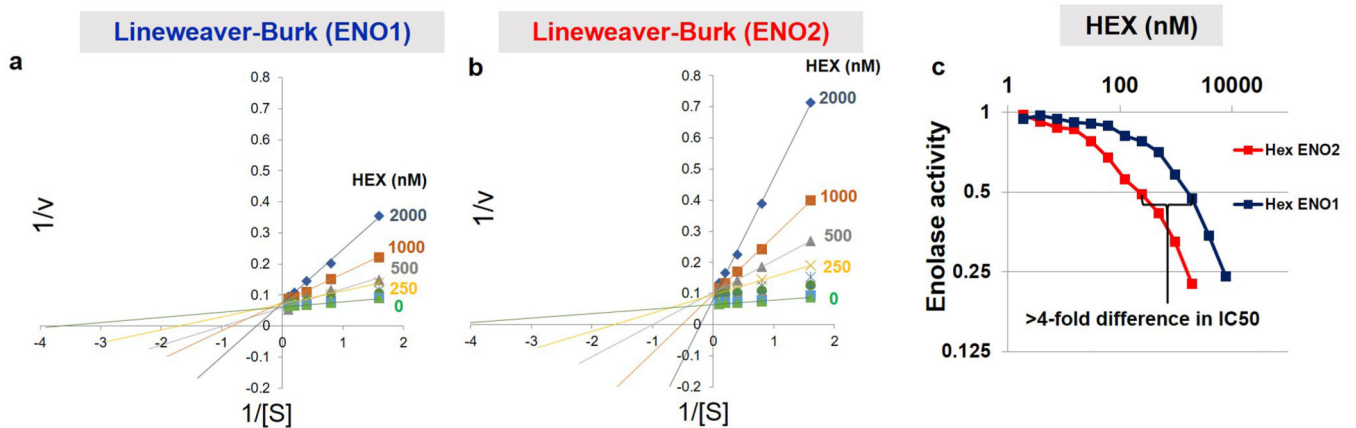
Statistical significance was analyzed using Microsoft Excel version 1902 or Prism GraphPad 8. Statistical tests used are indicated in the figure legends for each experiment. Additional information regarding statistics, software used, and study design is provided in the Reporting Summary

1. Extended Data



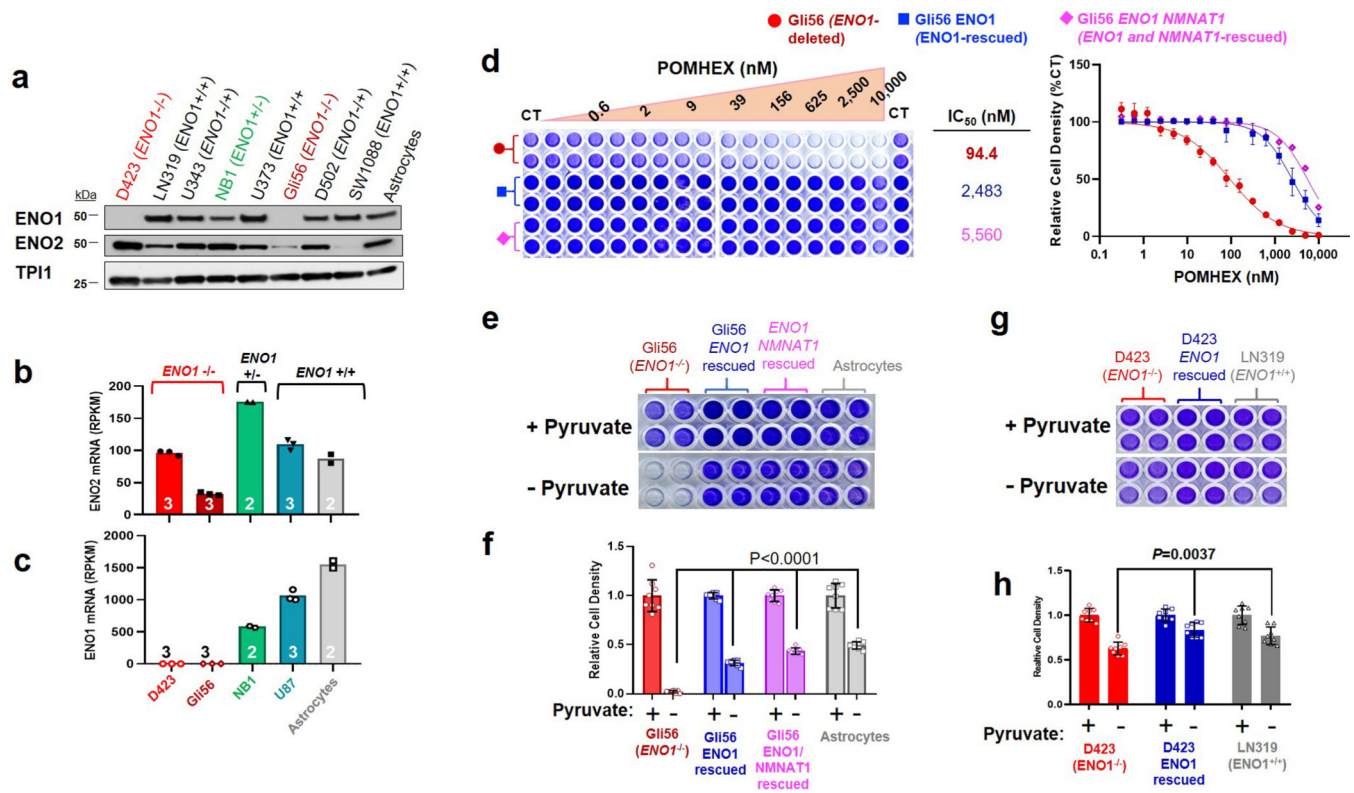
Extended Data Fig. 1. Rapid induction of anemia by non-ENO2-specific Enolase inhibitors

a. Non pro-drugged phosphonate Enolase inhibitors were administered to mice by tail vein IV injection at the times indicated (white arrows) to determine effects on hematocrit (fraction of RBC / total plasma volume). Each trace represents an individual mouse treated and sampled repeatedly over 10 days, with two animals per drug or vehicle (green). Phosphoacetylhydroxamate (PhAH; purple) caused a rapid and significant drop in hematocrit (and visible jaundice), which is then restored to initial levels after discontinuing treatment. PhAH is a pan-Enolase inhibitor with slightly greater potency against ENO1 over ENO2. As ENO1 is the sole isoform expressed in RBCs, anemia caused by PhAH is most likely due to on-target inhibitory activity against ENO1. **b.** Representative capillary tube after centrifugation from the hematocrit experiment described in **a**. The ratio of RBC fraction to total blood volume is decreased in response to PhAH treatment; pale yellow plasma in the PhAH sample indicates hemolysis. **c,d.** POMSF is a POM-pro-drug version of SF2312 that was generated for in vivo testing. Mice were IV tail vein injected with either vehicle (DMSO), POMSF, or POMHEX dissolved in PBS at the indicated doses. Capillary tubes were used to measure percent hematocrit. **c.** Hematocrit was determined as a function of time in response to Enolase inhibitors over a 10-day treatment course. Mice were administered either DMSO (green), POMSF (blue), or POMHEX (red) for 5 days before discontinuing treatment. Compared to the DMSO control and POMHEX, administration of POMSF results in decreased percent hematocrit, which is then restored to initial levels after discontinuing treatment. Significant differences by non-paired t-test with Bonferroni correction are indicated in **d**. **e.** Representative capillary tubes from mice treated with DMSO vehicle (left), POMSF (middle), and POMHEX (right). Note the decrease hematocrit (red bracket) as fraction of total blood volume (black bracket) from POMSF treatment; pale orange plasma indicates hemolysis



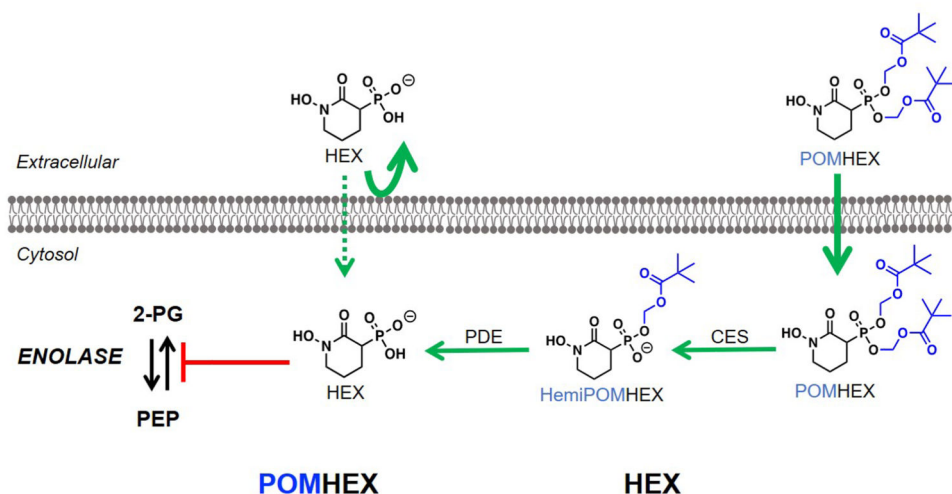
Extended Data Fig. 2. HEX is a substrate-competitive inhibitor with preference for ENO2
a, b. Enolase activity ($1/v$, y-axis) was measured spectrophotometrically *in vitro* using an NADH-coupled assay^{1,2}, with ENO1 and ENO2 activity plotted as a function of substrate concentration (x-axis, $1/S$: 2-phosphoglycerate in mM; HEX in nM). Data were plotted as Lineweaver-Burk with x-axis showing inverse of substrate versus inverse activity ($1/V$). Each dot represents on independent biochemical rate determination. Slopes (K_m -apparent/ V_{max}) were re-plotted as a function of inhibitor concentration in Figure 1c. **c.** Enolase

activity in lysates from ENO1 and ENO2 overexpressing D423 cells, measured as a function of HEX concentration; 0.5 mM 2-PG substrate concentration.



Extended Data Fig. 3. The Gli56 *ENO1*-homozygously deleted glioma cell line is sensitive to POMHEX and is pyruvate auxotrophic

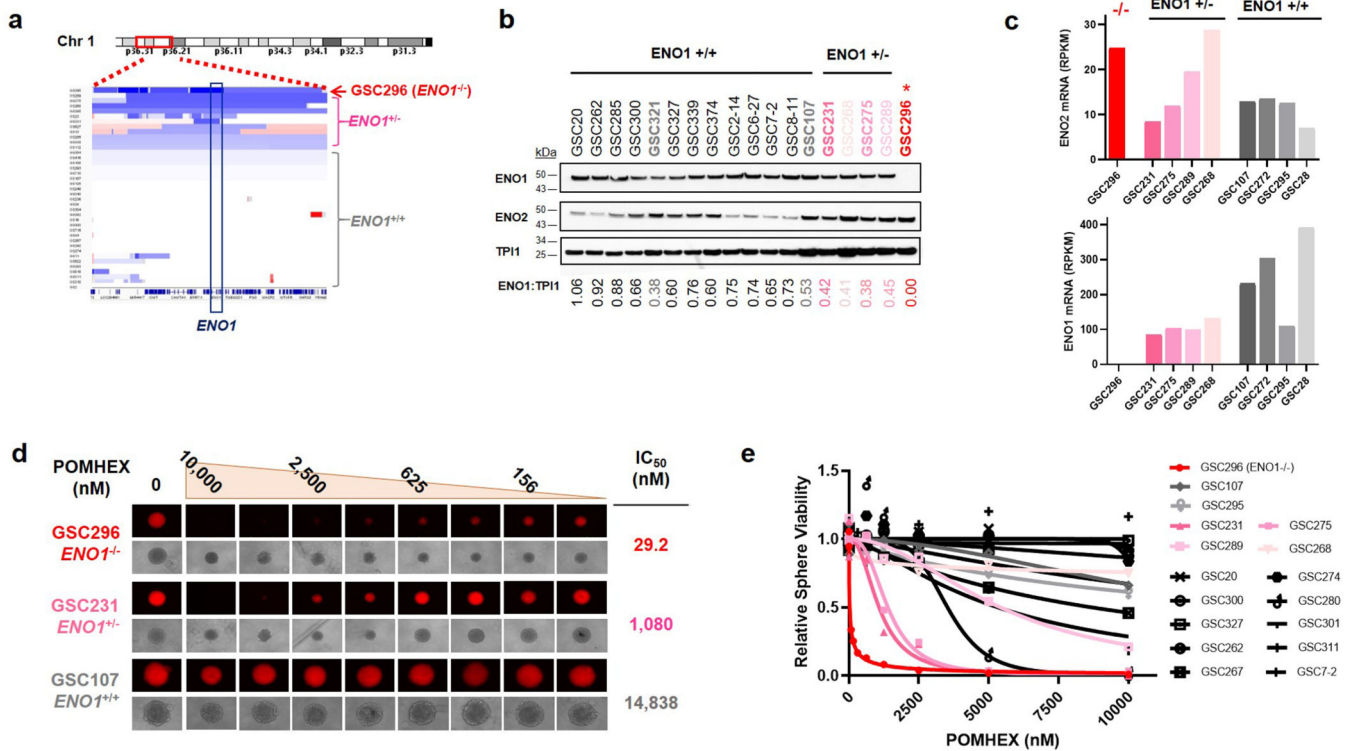
Sensitivity to POMHEX was determined in additional *ENO1*-homozygously deleted cell line, Gli56 (dark red) and its isogenic *ENO1*-rescued control^{3,4}. **a**. Absence of ENO1 protein confirmed by western blot in the Gli56 cell line; note levels of ENO2 are lower than in D423 (*ENO1*^{-/-}), which is confirmed by mRNA. **b**, **c**. RNA-seq mRNA expression of ENO1 and ENO2 in cell lines differing in *ENO1*-deletion status, confirming lower ENO2-expression in Gli56 compared to D423 cell. Each point represent one biological replicate, means are shown, n number is indicated for each cell line. **d**. Gli56 (dark red) is selectively sensitive to POMHEX compared to its isogenic *ENO1*-rescued control³ (blue). Another Gli56 rescued cell line (purple), in which *ENO1* and a neighboring deleted gene, *NMNAT1*, are re-expressed (generated for a separate collateral lethality project), also shows resistance to POMHEX. Cell density was visualized by crystal violet after 14 days of growth; fresh media (DMEM, contains 1.25 mM pyruvate) containing Enolase inhibitor was provided every 4 days (N = 4 biological replicates +/- S.E.M.). In contrast to the D423 cell line, Gli56 cannot be grown in pyruvate-free DMEM media, likely due to lower level of residual ENO2 expression. **e**, **f**. Gli56 *ENO1*-deleted, but not Gli56 *ENO1*-rescued cells, can grow in pyruvate-free DMEM. **g**, **h**. D423 *ENO1*-deleted cells can grow in pyruvate-free DMEM media, but slower than D423 *ENO1*-rescued or LN319 (*ENO1*-WT) cells. N = 8 biological replicates, mean +/- S.E.M. P value by 2-way ANOVA are indicated.



	POMHEX			HEX			Ratio IC ₅₀ POMHEX/HEX
	IC ₅₀ (nM)	Stdev	n	IC ₅₀ (nM)	Stdev	n	
D423 (<i>ENO1</i> -deleted)	35	19	12	1,875	431	6	53
D502 (<i>ENO1</i> -Heterozygous)	82	30	6	28,756	9,568	6	347
U343 (<i>ENO1</i> -Heterozygous)	559	335	6	19,723	10,675	7	35
D423 (<i>ENO1</i> -rescued)	2,261	941	6	163,943	56,412	3	72
LN319 (<i>ENO1</i> -WT)	1,328	355	8	229,037	57,772	7	172

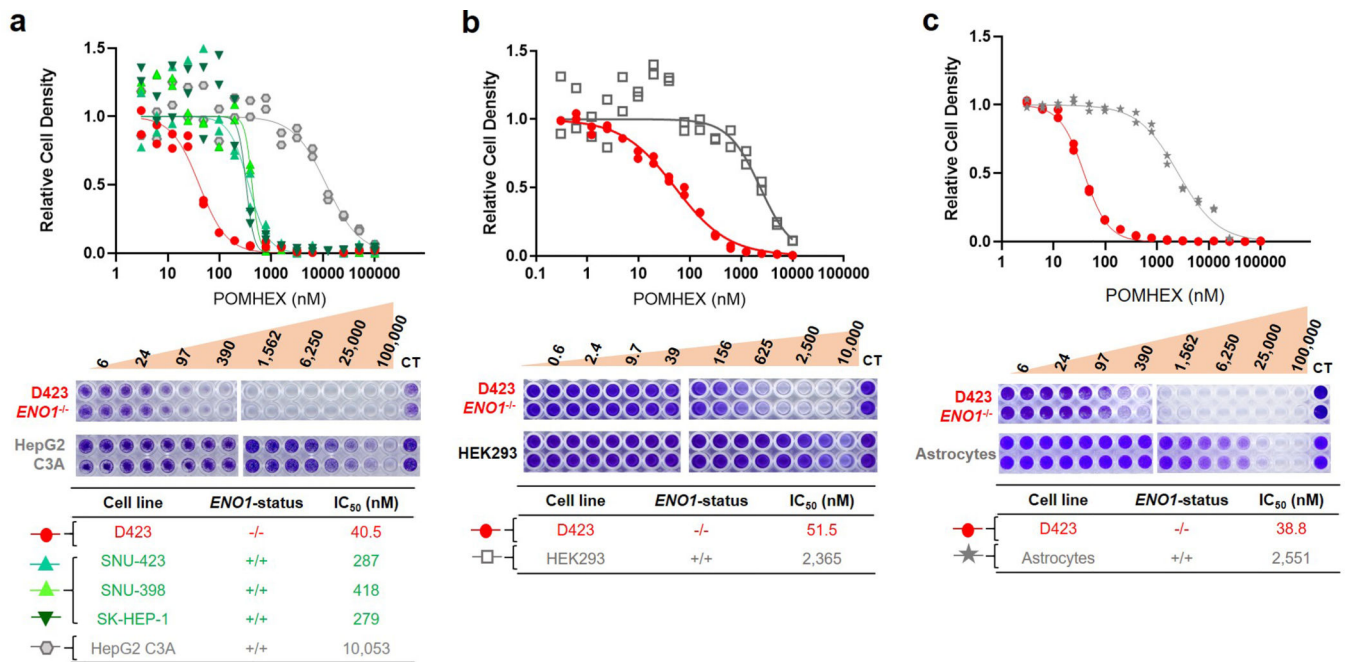
Extended Data Fig. 4. Relative sensitivities of glioma cell lines to the pro-drug POMHEX versus the active Enolase inhibitor HEX

Sensitivity of a panel of glioma cell lines with varying *ENO1* statuses to the Enolase inhibitors POMHEX and HEX. IC₅₀ values were calculated based on terminal cell density measured by crystal violet. D502 and U343 are *ENO1*-heterozygous deleted cell lines (~50% total Enolase^{3,4}). Consistent with our previous reports for pan-Enolase inhibitors^{3,4}, *ENO1*-homozygous deletion confers the greatest sensitivity to HEX, while *ENO1*-heterozygous deletion status shows intermediate sensitivity. While sensitivity to HEX is dependent on *ENO1*-deletion status, the sensitivity to POMHEX like depends not only on *ENO1*-deletion status but also expression of pro-drug bioactivation enzymes that transform POMHEX into active HEX enolase inhibitor (carboxylesterases, CES and phosphodiesterases, PDE). On average, the potency of POMHEX is ~75-fold greater than HEX though with substantial variation across cell lines. D502 is considerably more sensitive to POMHEX than U343 (IC₅₀ 82 vs 559 nM), yet U343 is more sensitive to HEX than D502 (IC₅₀ 19,723 nM vs 28,756 nM). This can be explained by higher levels of expression of pro-drug activating enzymes in the D502 glioma cell line result in greater sensitivity to POMHEX as compared to U343. Identification of the specific genes responsible, and their expression could be used for patient stratification, expanding the utility of Enolase inhibitors beyond those with *ENO1*-homozygous deletions.



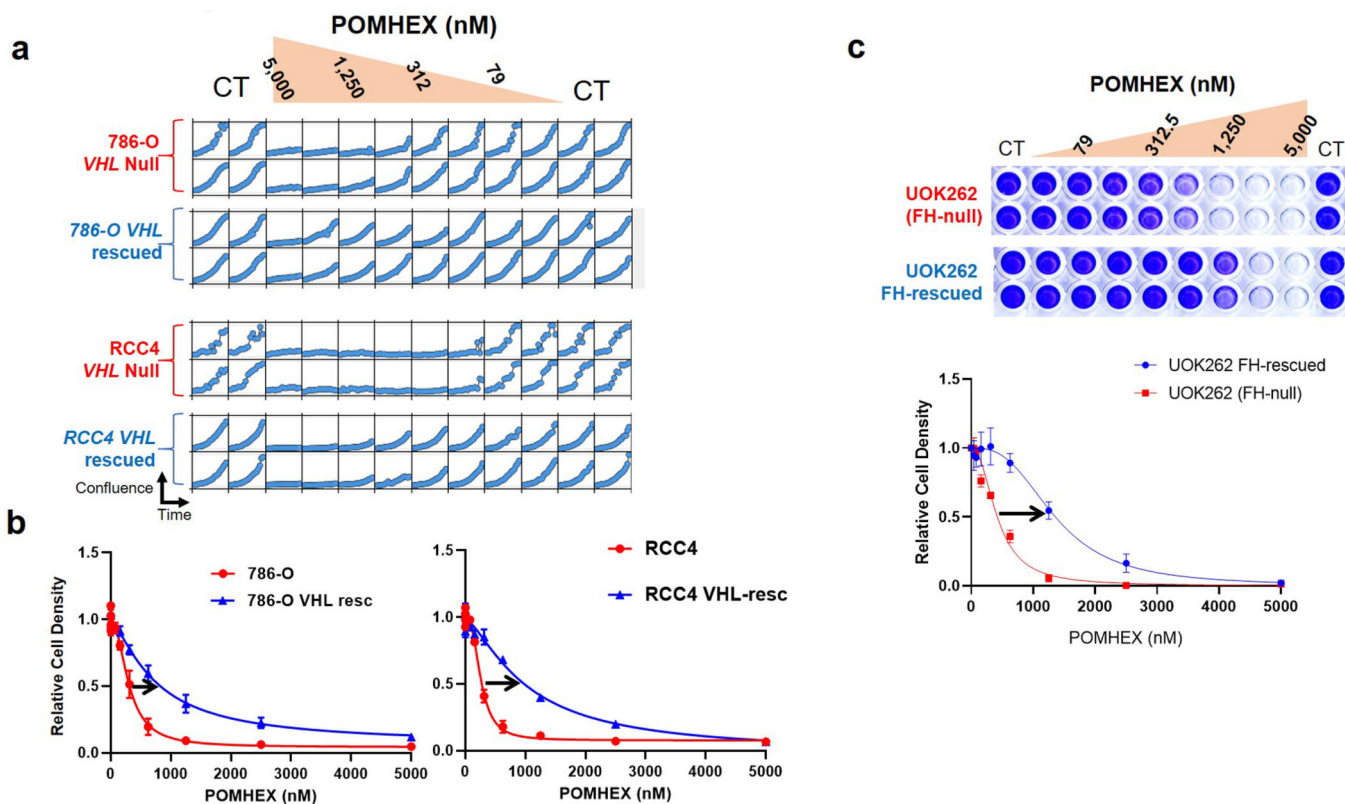
Extended Data Fig. 5. *ENO1*-deletion status predicts sensitivity to Enolase inhibitors in glioma sphere-forming cells (GSC)

GSCs and omics data were kindly shared by the Lang lab^{9,10}. **a.** Copy number variation at the 1p36 locus identifies GSC296 (red) as *ENO1*-homozygous deleted and GSC231, 268, 275, 289 as heterozygous deleted (pink). Dark blue regions represent bi-allelic (homozygous) deletion, while light blue regions correspond to mono-allelic loss. **b.** Confirmed lack of *ENO1* expression by western blot in GSC296 (red), with corresponding levels of *ENO2* shown. The western blot analysis for GSC296 was performed at least 3 times with similar outcomes. **c.** RNA-seq mRNA expression of *ENO1* (bottom) and *ENO2* (top) in *ENO1*-homozygous deleted and heterozygous deleted GSCs, confirming lack of *ENO1* expression. Each bar represents one biological replicate. **d,e.** Sensitivity of GSCs with varying *ENO1*-deletion status to POMHEX. Dissociated GSCs were seeded in 96-well round bottom-low attachment plates in duplicate and allowed to form spheroids. Spheroids were treated with a serial dilution of POMHEX for 1 week; media was changed every 3 days with fresh drug. Viability was visualized with 5 nM TMRE (red). TMRE was quantified by ImageJ and expressed as a function of vehicle controls. Each dot represents one biological replicate. GSC296 (*ENO1*^{-/-}) was distinctly sensitive to POMHEX. *ENO1*-heterozygous deleted GSCs showed intermediate sensitivity. *ENO1*-WT GSCs with the lowest residual *ENO2* expression showed the greatest sensitivity amongst *ENO1*-WT GSCs. Experiments with GSC296 were reproduced independently once.



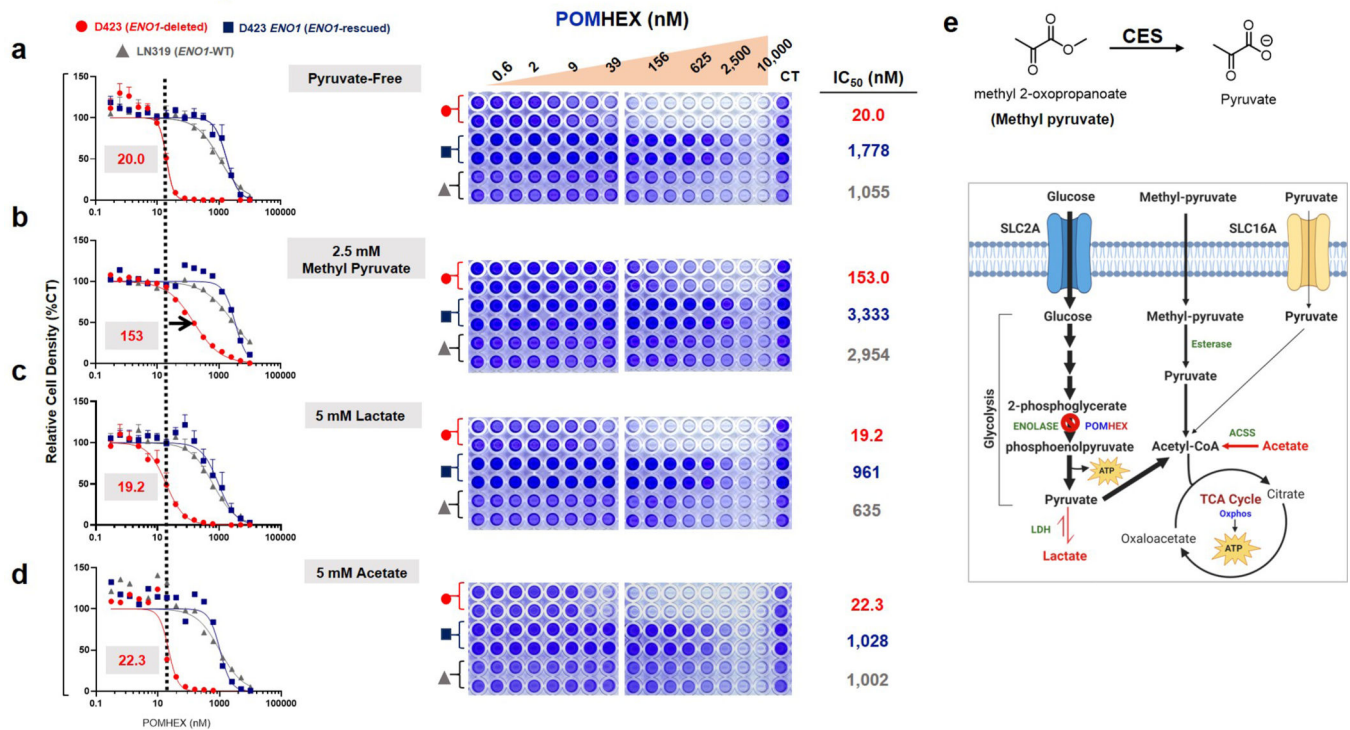
Extended Data Fig. 6. Normal and near-normal cell lines are minimally sensitive to POMHEX

All indicated cells were grown in RPMI and treated with a serial dilution of POMHEX for 5 days. Cell density was then quantified by crystal violet after 5 days of growth and expressed relative to control ($n = 2$ biological replicates). **a.** A panel of hepatocellular carcinoma cell lines (SNU-423, SNU-398, SK-HEP-1; grey) and highly differentiated, hepatoblastoma line (HepG2 C3A; blue) were treated with POMHEX; D423 (red) was tested as a point of reference. The IC₅₀ of POMHEX for most HCC cell lines is about 750 nM (grey), which is slightly lower than that for *ENO1*-WT glioma cell lines. However, the highly differentiated cell line, HepG2 C3A, was essentially insensitive with an IC₅₀ >10,000 nM. This resistance likely derives from the dependence of hepatocytes on OxPhos, with minimal requirements for glycolysis-derived ATP (excess ATP allows for glycolysis reversal, gluconeogenesis) and concurs with our data in NHP, which indicate no hepatotoxicity. **b.** HEK293 kidney cells (grey) are immortalized, non-transformed kidney cells. Sensitivity to POMHEX was comparable to that observed in *ENO1*-WT cancer cell lines. **c.** Non-immortalized human astrocytes (grey) showed IC₅₀ of >2,500 nM to POMHEX, which is also comparable to *ENO1*-WT glioma cell lines and far higher than that for *ENO1*-deleted D423 cells.



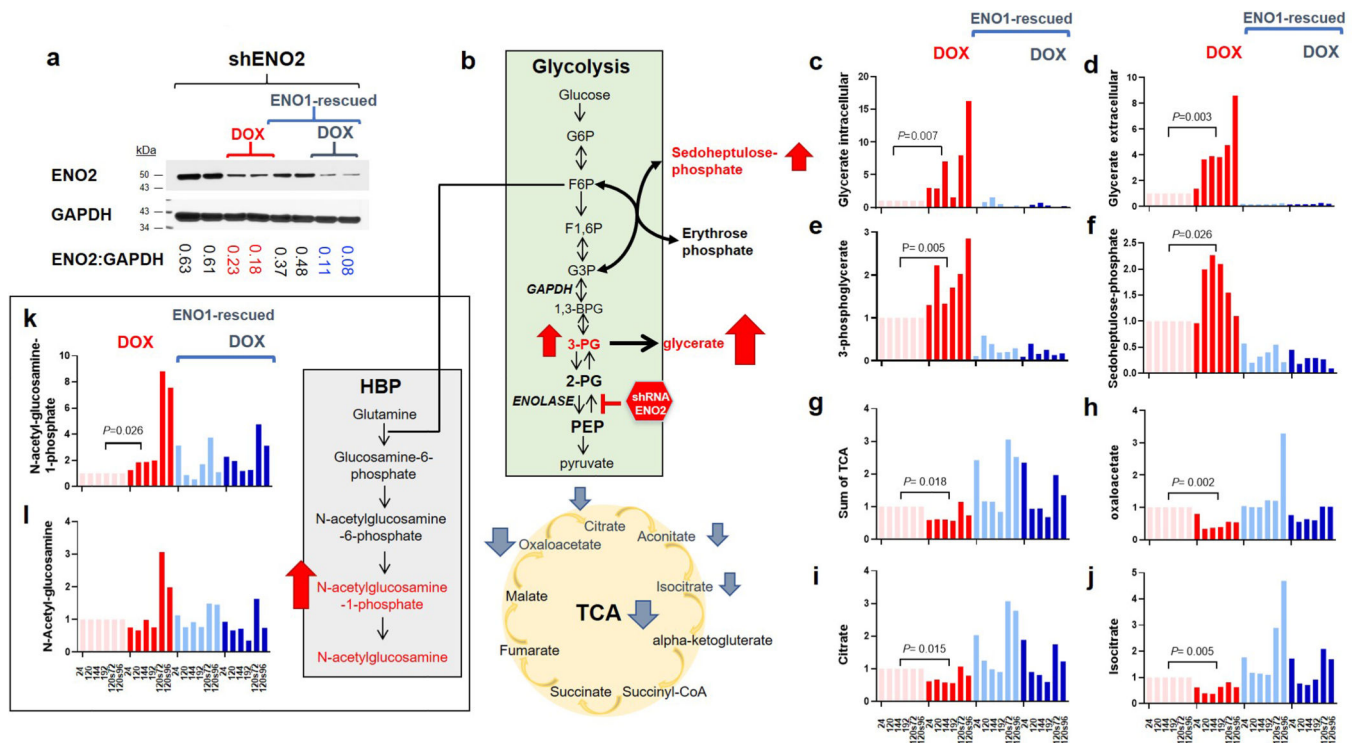
Extended Data Fig. 7. Utility of Enolase inhibitors beyond cancers with *ENO1*-deletions

Hyperactivation of HIF by loss of VHL tumor suppressor gene has been reported to sensitize cells to glycolysis inhibition¹². **a.** Proliferation of renal clear cell carcinoma cell lines that lack functional *VHL* (786-O and RCC4, red) and isogenic rescued cell lines re-expressing VHL (blue) was followed by Incucyte live cell imager (x-axis, time; y-axis, cell confluence) in response to POMHEX treatment. Each box represents one biological replicates. *VHL*-deleted parental lines showed 4- to 8-fold greater sensitivity than isogenic rescued VHL lines. **b.** Cell density quantified by crystal violet for the same cell lines corroborates Incucyte live imaging data (N = 4 biological replicates, with \pm S.E.M.). IC₅₀ for POMHEX in the RCC4 line is ~250 nM and 1,000 nM in the isogenic rescued line. TCA-cycle deficiency and defective oxidative phosphorylation by loss of function of Fumarase (*FH*) increase reliance on glycolysis and sensitize to glucose deprivation¹¹. **c.** Likewise, the *FH*-null renal carcinoma cell line, UOK262, (red) shows dramatically higher sensitivity to the Enolase inhibitor POMHEX than isogenic *FH*-rescued cell line control (blue). Cell density in response to POMHEX treatment was quantified by crystal violet (N = 4 biological replicates, with \pm S.E.M.).



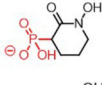
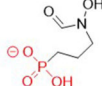
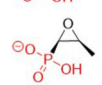
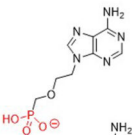
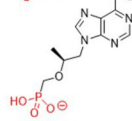
Extended Data Fig. 8. The synthetic cell permeable pyruvate pro-metabolite, methyl 2-oxopropanoate, significantly attenuates toxicity of POMHEX

ENO1-deleted (D423, red), *ENO1*-isogenically rescued (D423 *ENO1*, blue), and *ENO1*-WT (LN319, grey) cells were treated with POMHEX at the doses indicated (x-axis) in media (DMEM) free of pyruvate with either (a) 2.5 mM methyl 2-oxopropanoate “methyl pyruvate,” (b) 5 mM lactate, or (c) 5 mM acetate (d). Cell density after 5 days exposure was determined by crystal violet staining and expressed relative to non-drug contain controls (n = 4 biological replicates as indicated, +/ S.E.M.). The IC₅₀ for pyruvate-free media is indicated by a dashed line, for comparison. Exogenous methyl pyruvate attenuates sensitivity to Enolase inhibitors especially in *ENO1*-homozygously deleted cells (IC₅₀ shifted from ~20 nM to ~150 nM), but supplementation with lactate or acetate had minimal effects. (e) Methyl pyruvate is a cell-permeable, synthetic pro-metabolite of pyruvate that can passively diffuse into the cell without requiring monocarboxylate transporter (SLC16) activity. It can then be hydrolyzed by intracellular carboxylesterases to release pyruvate. While lactate and acetate could serve a similar purpose, the present data (c, d) suggest that the rate of acetyl-CoA production by these carbon sources is insufficient to compensate for loss of ATP and pyruvate by POMHEX-mediated inhibition of glycolysis.



Extended Data Fig. 9. ShRNA knockdown of ENO2 recapitulates metabolic disruptions caused by small-molecule ENO2 inhibitors

a. Knockdown of ENO2 by doxycycline-inducible shRNA in D423 *ENO1*-deleted and *ENO1*-rescued cells with the same constructs and cell lines used previously³. Induction of shENO2 results in ~70% decrease in ENO2-protein levels (ratios of band densities ENO2 to TPI, loading control, are indicated). The western blot analysis was performed once with each line representing a single biological replicate. Polar metabolites were profiled at specific times after induction of shENO2 with doxycycline (times indicated in x-axis, hours) in both conditioned media (extracellular) and cell pellet (intracellular), with cells passaged after 120 h. **b.** Schematic showing the Enolase reaction in the context of central carbon metabolism and associated pathways, with metabolites altered selectively in D423 *ENO1*-deleted cells in response to ENO2-knockdown. **c-e.** Accumulation of metabolites upstream of Enolase in response to ENO2-knockdown in *ENO1*-deleted but not *ENO1*-rescued cells recapitulates observation with Enolase inhibitors (Figure 4). Glycerate (**c, d**) was the most significantly altered metabolite in polar metabolomic profile of conditioned media in *ENO1*-deleted but not rescued cells. Intracellular glycerate levels (**c**) recapitulate this trend and mirror the levels of 3-PG(**e**), from which it is hydrolyzed. **f-j.** TCA-cycle metabolites were selectively decreased in response to ENO2-knockdown, recapitulating effects of small molecule Enolase inhibition (Figure 4). Similar to observations with small molecule Enolase inhibition, hexosamine biosynthesis pathway (HBP) metabolites increase in response to ENO2 knockdown. **k-l.** Each bar represents one biological replicate. *P* values from T-test of the log of the normalized values of each biological replicate are indicated.

Drug	Plasma Elimination Half-Lives				References
					
 HEX	6 min (mouse)	~60 min (predicted)	61 min	~100 min (predicted)	This work
 Fosmidomycin	16 min (rat)	67 min	N/A	99 min	51
 Fosfomycin	28 min (rat)	78 min	N/A	90 -120 min	48-51
 Adefovir	9 min (mouse)	396 ± 24 min (terminal)	47 min	99 min	28, 46
 Tenofovir	30 ± 12 min (mouse)	60-90 min 600 min (terminal)	90-210 min	~120 min	41-46

Extended Data Fig. 10. Phosphonate-containing drugs show similar, species-specific pharmacokinetics

The PK properties of phosphonate containing drugs have been well-studied in diverse model species as well as human patients and exhibit remarkable similarity, despite extensive chemical diversity. The very similar PK properties of these diverse drugs, derives from the fact their physiochemistry and pharmacokinetics are predominantly dictated by the negatively charged phosphonate group, conferring water solubility and limited protein binding. This water solubility means that drugs distribute with water and are cleared by a predominantly renal mechanism. Renal excretion is passive glomerular filtration and active tubular secretion, which can be modulated by drugs like Probenecid⁴⁰. Rodent species rapidly eliminate phosphonate drugs, with >95% of injected drug excreted unchanged within 1 hr. In non-human primates, half-lives are typically 10-times longer, and in human patients even more so. This copious body of PK data provides a guide towards predictions of how HEX might behave in human patients. The comparison with fosmidomycin is especially informative as it is nearly identical, except for 1 C-C bond, to fosmidomycin. The elimination half-life of HEX in rodents and NHP falls very much in line with other phosphonate drugs and allows reasonable confidence in PK prediction in other models (canines) and in human patients. N/A = data not found in the literature.

Supplementary Material

Refer to Web version on PubMed Central for supplementary material.

ACKNOWLEDGEMENTS.

We thank Steven Millward, Seth Gammon, Fred Lang, David Pwinica-Worms, John De Groot, Peter Cserjesi, Christopher Halbrook, Costas Lyssiotis and Jason Huse for critical comments and suggestions. We thank Hannah Butterfield, Lexiah Jacobs, Anton Portal, Prakriti Shresta, Mykia Washington and Pornpa Suriyamongkol for technical assistance. We thank James Holton and George Meigs for their assistance with X-ray diffraction data collection. We thank Kumar Kalurachchi and John McMurray for assistance with NMR. The UT MD Anderson Cancer Center NMR Core Facility is supported in part by the NCI Cancer Center Support Grant (CA16672). We thank Min Yuan and Susanne Breitkopf for help with the mass spectrometry experiments. We thank Zhiqiang (George) Jia for technical support with NHP experiments at CRL. We thank James Long for help with statistical analysis and for critical reading. We thank Keith Michel, Charles Kingsley, Vivien Tran and the rest of the SAIF team for expert assistance with MRI imaging; Ganesh Rao, Verlene Henry, Joy Gumin and Fred Lang for GSC's and intracranial cell implantations. The Pharmaceutical Chemistry Facility and the Small Animal Imaging Facility at The UT MD Anderson Cancer Center were supported by the NIH/NCI Cancer Center Support Grant under award number P30CA016672. Financial support was provided by NIH CDP SPORE P50CA127001-07 (F.L.M.), NIH SPORE 2P50CA127001-11A1 (F.L.M.), ACS RSG-15-145-01-CDD (F.L.M.), NCCN YIA170032 (F.L.M. Young Investigator Award), The Andrew Sabin Family Foundation (F.L.M. Fellow award), The Dr. Marnie Rose Foundation (F.L.M.), The Uncle Kory Foundation (F.L.M.), and The University of Texas MD Anderson Cancer Center Institutional Research Grant (F.L.M.), CPRIT RP140612 (R.A.D.) and NIH R01 CA225955 (R.A.D.). This work is dedicated to the memory of Dr. John Stuart McMurray, an expert in phosphonate pro-drug synthesis, without whom this would not have been possible.

REFERENCES.

1. Fonvielle M, Mariano S. & Therisod M. New inhibitors of rabbit muscle triose-phosphate isomerase. *Bioorganic Med. Chem. Lett.* 15, 2906–2909 (2005).
2. Anderson VE, Weiss PM & Cleland WW Reaction Intermediate Analogues for Enolase. *Biochemistry* 23, 2779–2786 (1984). [PubMed: 6380574]
3. Muller FL et al. Passenger deletions generate therapeutic vulnerabilities in cancer. *Nature* 488, 337–343 (2012). [PubMed: 22895339]
4. Leonard PG et al. SF2312 is a natural phosphonate inhibitor of enolase. *Nat. Chem. Biol.* 12, 1053–1058 (2016). [PubMed: 27723749]
5. P B-H et al. Decreased red cell enolase activity in a 40-year-old woman with compensated haemolysis. *Scand. J. Haematol.* 33, 401–404 (1984). [PubMed: 6515323]
6. Stefanini M. Chronic Hemolytic Anemia Associated with Erythrocyte Enolase Deficiency Exacerbated by Ingestion of Nitrofurantoin. *Am. J. Clin. Pathol.* 58, 408–414 (1972). [PubMed: 4640298]
7. Muller F. et al. WO2016145113A1 - Enolase inhibitors and methods of treatment therewith. (2016).
8. Krucinska J. et al. Structural and Functional Studies of Bacterial Enolase, a Potential Target against Gram-Negative Pathogens. *Biochemistry* 58, 1188–1197 (2019). [PubMed: 30714720]
9. H J. et al. Examination of the Therapeutic Potential of Delta-24-RGD in Brain Tumor Stem Cells: Role of Autophagic Cell Death. *J. Natl. Cancer Inst.* 99, (2007).
10. J F. et al. Exosomes From Glioma-Associated Mesenchymal Stem Cells Increase the Tumorigenicity of Glioma Stem-like Cells via Transfer of miR-1587. *Cancer Res.* 77, (2017).
11. Y Y. et al. UOK 262 Cell Line, Fumarate Hydratase Deficient (FH-/FH-) Hereditary Leiomyomatosis Renal Cell Carcinoma: In Vitro and in Vivo Model of an Aberrant Energy Metabolic Pathway in Human Cancer. *Cancer Genet. Cytogenet.* 196, (2010).
12. DA C. et al. Targeting GLUT1 and the Warburg Effect in Renal Cell Carcinoma by Chemical Synthetic Lethality. *Sci. Transl. Med.* 3, (2011).
13. Pradere U, Garnier-Amblard EC, Coats SJ, Amblard F. & Schinazi RF Synthesis of Nucleoside Phosphate and Phosphonate Prodrugs. *Chem. Rev.* 114, 9154–9218 (2014). [PubMed: 25144792]
14. Foster KJ et al. Blood intermediary metabolite and insulin concentrations after an overnight fast: reference ranges for adults, and interrelations. *Clin. Chem.* 24, (1978).
15. Vasconcelos-dos-Santos A. et al. Biosynthetic machinery involved in aberrant glycosylation: Promising targets for developing of drugs against cancer. *Frontiers in Oncology* vol. 5 (2015).
16. Tarrado-Castellarnau M, de Atauri P. & Cascante M. Oncogenic regulation of tumor metabolic reprogramming. *Oncotarget* vol. 7 62726–62753 (2016).

17. Pantelouris EM Absence of thymus in a mouse mutant. *Nature* vol. 217 370–371 (1968). [PubMed: 5639157]
18. Farquhar D, Khan S, Srivastva DN & Saunders PP Synthesis and antitumor evaluation of bis[(pivaloyloxy)methyl] 2'-deoxy-5-fluorouridine 5'-monophosphate (FdUMP): a strategy to introduce nucleotides into cells. *J. Med. Chem.* 37, 3902–9 (1994). [PubMed: 7966151]
19. Duysen EG et al. Production of ES1 Plasma Carboxylesterase Knockout Mice for Toxicity Studies. *Chem. Res. Toxicol.* 24, 1891–1898 (2011). [PubMed: 21875074]
20. Rudakova EV, Boltneva NP & Makhaeva GF Comparative Analysis of Esterase Activities of Human, Mouse, and Rat Blood. *Bull. Exp. Biol. Med.* 152, 73–75 (2011). [PubMed: 22803044]
21. Bahar FG, Ohura K, Ogihara T. & Imai T. Species Difference of Esterase Expression and Hydrolase Activity in Plasma. *J. Pharm. Sci.* 101, 3979–3988 (2012). [PubMed: 22833171]
22. Yan VC & Muller FL Advantages of the Parent Nucleoside GS-441524 over Remdesivir for Covid-19 Treatment. *ACS Med. Chem. Lett.* 11, 1361–1366 (2020). [PubMed: 32665809]
23. Humle N. et al. Targeted Vascular Drug Delivery in Cerebral Cancer. *Curr. Pharm. Des.* 22, 5487–5504 (2016). [PubMed: 27464719]
24. JF, de G. & WK Y. Bevacizumab and Irinotecan in the Treatment of Recurrent Malignant Gliomas. *Cancer J.* 14, (2008).
25. Nau R, Sörgel F. & Eiffert H. Penetration of drugs through the blood-cerebrospinal fluid/blood-brain barrier for treatment of central nervous system infections. *Clin. Microbiol. Rev.* 23, 858–83 (2010). [PubMed: 20930076]
26. Brunner M. et al. Penetration of fosfomycin into the parenchyma of human brain: a case study in three patients. *Br. J. Clin. Pharmacol.* 54, 548–50 (2002).
27. Pfeifer G, Frenkel C. & Entzian W. Pharmacokinetic aspects of cerebrospinal fluid penetration of fosfomycin. *Int. J. Clin. Pharmacol. Res.* 5, 171–4 (1985). [PubMed: 4018950]
28. Naesens L, Balzarini J, Bischofberger N. & De Clercq E. Antiretroviral Activity and Pharmacokinetics in Mice of Oral Bis(Pivaloyloxymethyl)-9-(2-Phosphonylmethoxyethyl)Adenine, the Bis(Pivaloyloxymethyl) Ester Prodrug of 9-(2-Phosphonylmethoxyethyl)Adenine. *Antimicrob. Agents Chemother.* 40, 22–28 (1996). [PubMed: 8787873]
29. KK VR et al. Biological effects of short-term or prolonged administration of 9-[2-(phosphonomethoxy)propyl]adenine (tenofovir) to newborn and infant rhesus macaques. *Antimicrob. Agents Chemother.* 48, 1469–1487 (2004). [PubMed: 15105094]
30. Bahar FG, Ohura K, Ogihara T. & Imai T. Species Difference of Esterase Expression and Hydrolase Activity in Plasma. *J. Pharm. Sci.* 101, 3979–3988 (2012). [PubMed: 22833171]
31. Lockie F. Ifosfamide: pharmacokinetic properties for central nervous system metastasis prevention. *Ann. Oncol.* 17, (2006).
32. Benito J. et al. Hypoxia-activated prodrug TH-302 targets hypoxic bone marrow niches in pre-clinical leukemia models. *Clin. Cancer Res.* 22, 1687–1698 (2016). [PubMed: 26603259]
33. Beran M, Andersson BS, Wang Y, McCredie KB & Farquhar D. The Effects of Acetaldophosphamide, a Novel Stable Aldophosphamide Analogue, on Normal Human and Leukemic Progenitor Cells in Vitro: Implications for Use in Bone Marrow Purging. *Cancer Res.* 48, (1988).
34. Ludeman SM The Chemistry of the Metabolites of Cyclophosphamide. *Curr. Pharm. Des.* 5, 627–643 (1999). [PubMed: 10469895]
35. Mazur L, Opyodo-Chanek M, Stojak M. & Wojcieszek K. Mafosfamide as a New Anticancer Agent: Preclinical Investigations and Clinical Trials. *Anticancer Res.* 32, 2783–2789 (2012). [PubMed: 22753738]
36. Guise CP et al. Bioreductive Prodrugs as Cancer Therapeutics: Targeting Tumor Hypoxia. *Chin. J. Cancer* 33, 80–86 (2014). [PubMed: 23845143]
37. Mazur L, Opyodo-Chanek M. & Stojak M. Glufosfamide as a New Oxazaphosphorine Anticancer Agent. *Anticancer Drugs* 22, 488–493 (2011). [PubMed: 21427562]
38. Tobias C, S. & F. Borch, R. Synthesis and Biological Studies of Novel Nucleoside Phosphoramidate Prodrugs. *J. Med. Chem.* 44, 4475–4480 (2001). [PubMed: 11728193]

39. Wu W, Sigmond J, J. Peters G & F. Borch R. Synthesis and Biological Activity of a Gemcitabine Phosphoramidate Prodrug. *J. Med. Chem.* 50, 3743–3746 (2007). [PubMed: 17602464]
40. Lacy SA, M Hitchcock MJ, Lee WA, Telliart P. & Cundy KC Effect of Oral Probenecid Coadministration on the Chronic Toxicity and Pharmacokinetics of Intravenous Cidofovir in Cynomolgus Monkeys Effect of Oral Probenecid Coadministration on the Chronic Toxicity and Pharmacokinetics of Intravenous Cidofovir in Cyno-molgus Monkeys. *TOXICOLOGICAL SCIENCES* vol. 44 <https://academic.oup.com/toxsci/article/44/2/97/1611572> (1998).
41. Van Rompay KKA, Hamilton M, Kearney B. & Bischofberger N. Pharmacokinetics of tenofovir in breast milk of lactating Rhesus macaques. *Antimicrob. Agents Chemother.* 49, 2093–2094 (2005). [PubMed: 15855535]
42. Van Rompay KKA et al. Biological effects of short-term or prolonged administration of 9-[2-(phosphonomethoxy)propyl]adenine (tenofovir) to newborn and infant rhesus macaques (*Antimicrobial Agents and Chemotherapy* (2004) 48, 5 (1469–1487)). *Antimicrobial Agents and Chemotherapy* vol. 48 2346 (2004).
43. Naesens L. et al. Antiretroviral efficacy and pharmacokinetics of oral bis(isopropylloxycarbonyloxymethyl)-9-(2-phosphonylmethoxypropyl)adenine in mice. *Antimicrob. Agents Chemother.* 42, 1568–1573 (1998). [PubMed: 9660984]
44. Duwal S, Schütte C. & von Kleist M. Pharmacokinetics and pharmacodynamics of the reverse transcriptase inhibitor tenofovir and prophylactic efficacy against HIV-1 infection. *PLoS One* 7, e40382 (2012).
45. Deeks SG et al. Safety, pharmacokinetics, and antiretroviral activity of intravenous 9- [2-(R)-(phosphonomethoxy)propyl]adenine, a novel anti-human immunodeficiency virus (HIV) therapy, in HIV-infected adults. *Antimicrob. Agents Chemother.* 42, 2380–2384 (1998). [PubMed: 9736567]
46. Cundy KC et al. Pharmacokinetics and bioavailability of the anti-human immunodeficiency virus nucleotide analog 9-[(R)-2-(phosphonomethoxy)propyl]adenine (PMPA) in dogs. *Antimicrob. Agents Chemother.* 42, 687–690 (1998). [PubMed: 9517952]
47. Naesens L, Balzarini J, Bischofberger N. & De Clercq E. Antiretroviral activity and pharmacokinetics in mice of oral bis(pivaloyloxymethyl)-9-(2-phosphonylmethoxyethyl)adenine, the bis(pivaloyloxymethyl) ester prodrug of 9-(2-phosphonylmethoxyethyl)adenine. *Antimicrob. Agents Chemother.* 40, 22–28 (1996). [PubMed: 8787873]
48. Zykov IN et al. Pharmacokinetics and pharmacodynamics of fosfomycin and its activity against extended-spectrum-lactamase-, plasmid-mediated AmpC-, and carbapenemase-producing *Escherichia coli* in a murine urinary tract infection model. *Antimicrob. Agents Chemother.* 62, (2018).
49. Pérez DS, Tapia MO & Soraci AL Fosfomycin: Uses and potentialities in veterinary medicine. *Open Vet. J.* 4, 26–43 (2014). [PubMed: 26623336]
50. Kirby WMM Pharmacokinetics of fosfomycin. *Chemotherapy* 23, 141–151 (1977). [PubMed: 832510]
51. Murakawa T, Sakamoto H, Fukada S, Konishi T. & Nishida M. Pharmacokinetics of fosmidomycin, a new phosphonic acid antibiotic. *Antimicrob. Agents Chemother.* 21, 224–230 (1982). [PubMed: 7073262]
52. Sjövall J, Bergdahl S, Movin G, Ogenstad S. & Saarimäki M. Pharmacokinetics of foscarnet and distribution to cerebrospinal fluid after intravenous infusion in patients with human immunodeficiency virus infection. *Antimicrob. Agents Chemother.* 33, 1023–1031 (1989). [PubMed: 2528939]
53. Wager TT, Hou X, Verhoest PR & Villalobos A. Central Nervous System Multiparameter Optimization Desirability: Application in Drug Discovery. *ACS Chem. Neurosci* 7, 3 (2016).
54. Borch RF et al. Synthesis and Evaluation of Nitroheterocyclic Phosphoramidates as Hypoxia-Selective Alkylating Agents. *J. Med. Chem.* 43, 2258–2265 (2000). [PubMed: 10841804]
55. Yan VC et al. Bioreducible Phosphonoamidate Pro-drug Inhibitor of Enolase: Proof of Concept Study. *ACS Med. Chem. Lett.* 11, 1484–1489 (2020). [PubMed: 32676158]

56. Valk PE, Mathis CA, Prados MD, Gilbert JC & Budinger TF Hypoxia in human gliomas: demonstration by PET with fluorine-18-fluoromisonidazole. *J. Nucl. Med.* 33, 2133–7 (1992). [PubMed: 1334136]
57. Yan VC, Pham C-D & Muller FL Expedient Method for Direct Mono-amidation of Phosphonic and Phosphoric Acids. *ChemRxiv* (2020) doi:10.26434/CHEMRXIV.12073131.V1.
58. Yan VC, Pham C-D, Arthur K. & Muller FL Aliphatic Amines are Viable Pro-drug Moieties in Phosphonoamidate Drugs. *bioRxiv* 2020.04.05.026583 (2020) doi:10.1101/2020.04.05.026583.
59. JF P. et al. A Unique Model for SDH-deficient GIST: An Endocrine-Related Cancer. *Endocr. Relat. Cancer* 25, 943–954 (2018). [PubMed: 29967109]
60. Maitiuhoheti M. et al. Enhancer Reprogramming Confers Dependence on Glycolysis and IGF signaling in KMT2D Mutant Melanoma. *bioRxiv* 507327 (2018) doi:10.1101/507327.
61. Alam H. et al. Super-enhancer impairment is a link between MLL4-inactivated lung tumors and their vulnerability to glycolysis pathway inhibition. *bioRxiv* 507202 (2018) doi:10.1101/507202.
62. MS G. Glucose Sensing in Pancreatic Islet Beta Cells: The Key Role of Glucokinase and the Glycolytic Intermediates. *Proc. Natl. Acad. Sci.* 90, (1993).
63. DO G. et al. Non-enzymatic Lysine Lactoylation of Glycolytic Enzymes. *Cell Chem. Biol.* 27, 206–213 (2020). [PubMed: 31767537]
64. Muller F, Muller F, Aquilanti E. & DePinho R. In vitro enzymatic activity assay for ENOLASE in mammalian cells in culture. *Nat. Protoc. Exch.* (2012) doi:10.1038/protex.2012.040.
65. Gillies RJ, Didier N. & Denton M. Determination of cell number in monolayer cultures. *Anal. Biochem.* 159, 109–13 (1986). [PubMed: 3812988]
66. Kueng W, Silber E. & Eppenberger U. Quantification of cells cultured on 96-well plates. *Anal. Biochem.* 182, 16–9 (1989). [PubMed: 2604040]
67. Bady P. et al. DNA fingerprinting of glioma cell lines and considerations on similarity measurements. *Neuro. Oncol.* 14, 701–711 (2012). [PubMed: 22570425]
68. Parsons DW et al. An Integrated Genomic Analysis of Human Glioblastoma Multiforme. *Science* (80-.). 321, 1807–1812 (2008).
69. Nistér M. et al. Evidence for progression changes in the human malignant glioma line U-343 MGa: analysis of karyotype and expression of genes encoding the subunit chains of platelet-derived growth factor. *Cancer Res.* 47, 4953–60 (1987). [PubMed: 3497714]
70. Lal S. et al. An implantable guide-screw system for brain tumor studies in small animals. *J. Neurosurg.* 92, 326–333 (2000). [PubMed: 10659021]
71. Yuan M, Breitkopf SB, Yang X. & Asara JM A positive/negative ion-switching, targeted mass spectrometry-based metabolomics platform for bodily fluids, cells, and fresh and fixed tissue. *Nat. Protoc.* 7, 872–881 (2012). [PubMed: 22498707]
72. Geoff T. et al. Biological Crystallography iMOSFLM: a new graphical interface for diffraction-image processing with MOSFLM. *Acta Crystallogr. Sect. D Biol. Crystallogr.* 67, 271–281 (2011). [PubMed: 21460445]
73. Evans PR & Murshudov GN How good are my data and what is the resolution? *Acta Crystallogr. Sect. D Biol. Crystallogr.* 69, 1204–1214 (2013). [PubMed: 23793146]
74. Emsley P, Lohkamp B, Scott WG & Cowtan K. Features and development of Coot. *Acta Crystallogr. Sect. D Biol. Crystallogr.* 66, 486–501 (2010). [PubMed: 20383002]
75. Afonine PV et al. Towards automated crystallographic structure refinement with phenix.refine. *Acta Crystallogr. Sect. D Biol. Crystallogr.* 68, 352–367 (2012). [PubMed: 22505256]
76. Adams PD et al. PHENIX: a comprehensive Python-based system for macromolecular structure solution. *Acta Crystallogr. Sect. D Biol. Crystallogr.* 66, 213–21 (2010). [PubMed: 20124702]

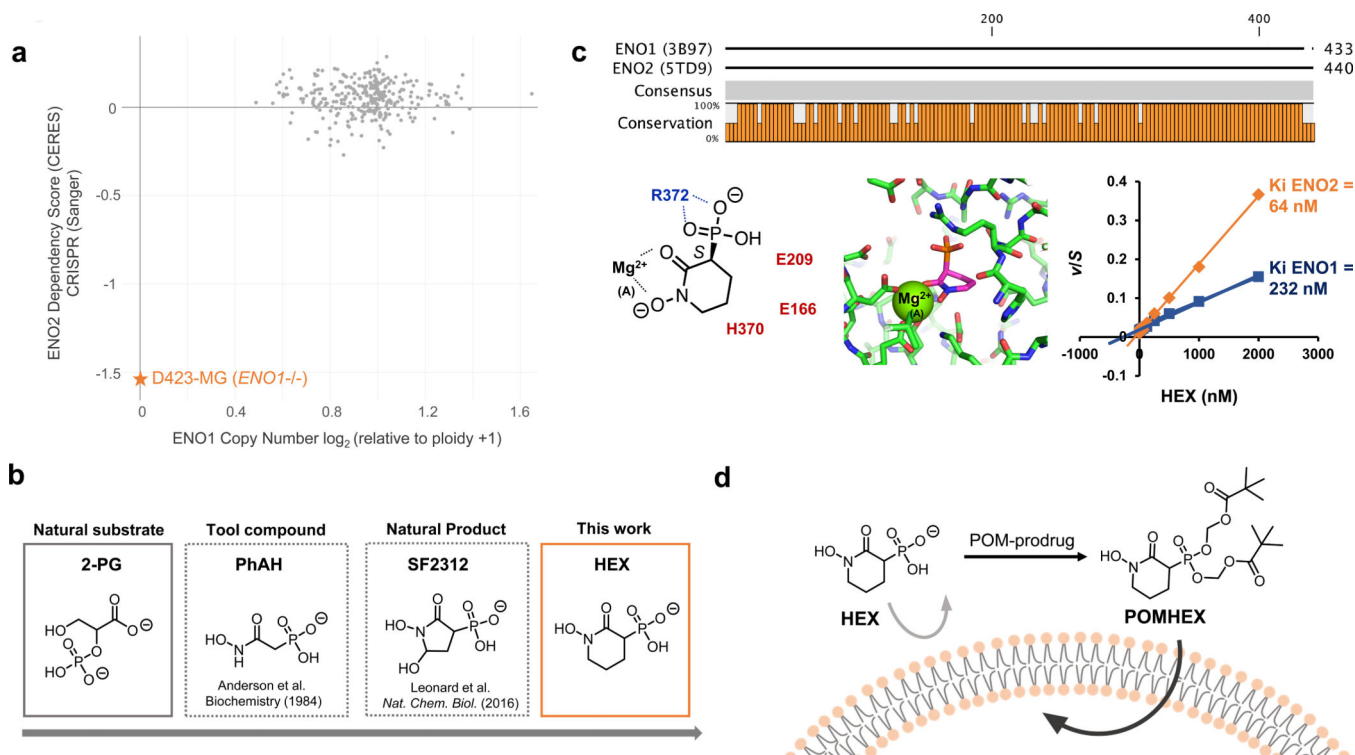


Figure 1. HEX is a substrate-competitive inhibitor of Enolase with specificity for ENO2.

a. Cells with ENO1 homozygous deletions (e.g. D423) are highly dependent on ENO2 to perform glycolysis, as indicated by the ENO2 CERES score. Plot adapted from the Cancer Dependency Map. **b.** Timeline on the development of ENO2-specific Enolase inhibitors. **c.** HEX displays ~4-fold specificity for ENO2 over ENO1 despite their structural similarities. Co-crystal structure of HEX and ENO2 (PDB: 5IDZ) indicates that the carbonyl and hydroxamate are crucial for chelating to the active site Mg^{2+} while the anionic phosphonate forms a salt bridge with R372. HEX shows competitive Michealis-Menten kinetics; plot of apparent K_m/V_{max} (from Supplementary Figure S1) as a function of HEX concentration (x-axis) for ENO1 and ENO2. **d.** HEX was modified with POM pro-drug groups to enhance its cell- and blood-brain-barrier permeability.

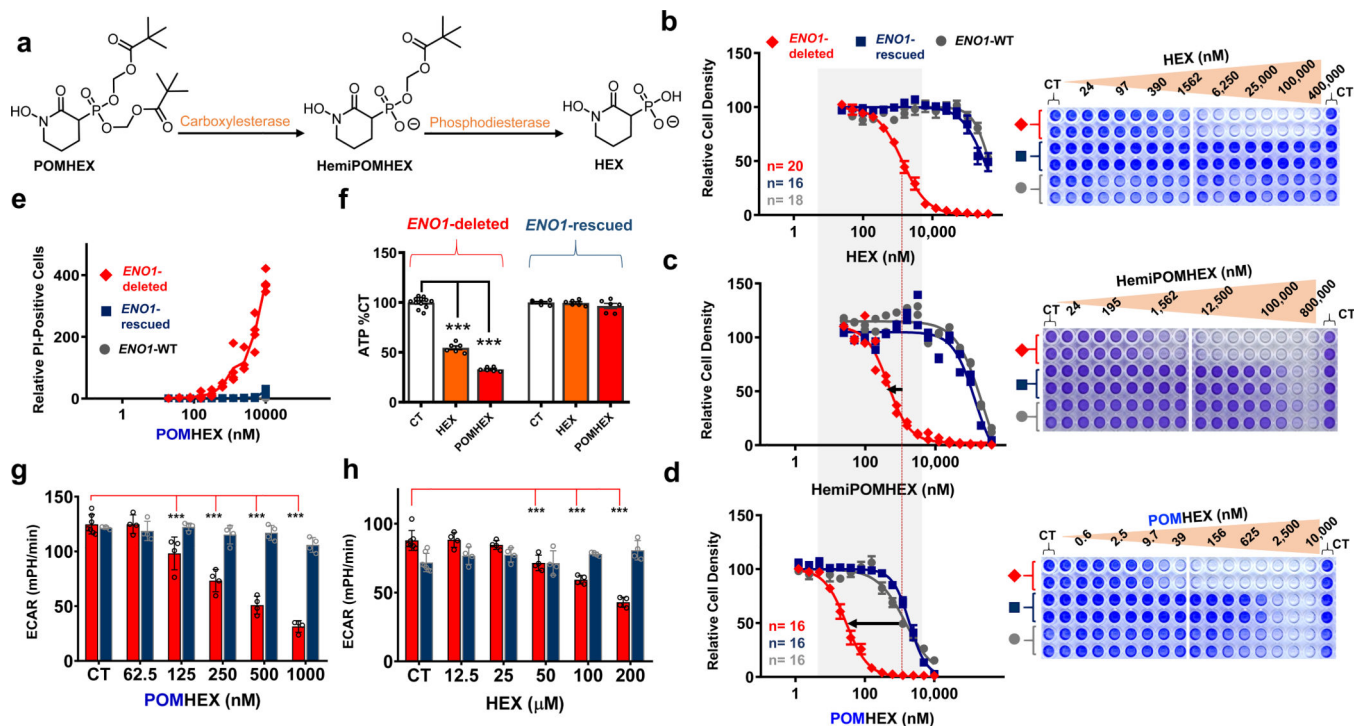


Figure 2. POMHEX is a potent pro-drug inhibitor of ENO2.

a. Proposed mechanism of bioactivation. Hydrolysis of the first POM group occurs through carboxylesterases while hydrolysis of the second POM group occurs through phosphodiesterases. **b-d.** POM groups improve the cellular permeability of HEX as indicated by left-shift in IC₅₀s for HemiPOMHEX and POMHEX. POMHEX is > 40-fold more potent than the non-pro-drug HEX (**b** versus **d**). Selective action against *ENO1*-deleted cells (D423, red) over *ENO1*-isogenically rescued (D423 *ENO1*, blue), and *ENO1*-WT (LN319, grey) cells is maintained. Number of independent experiments (n) is indicated in **b** and **d** for each cell line, mean ± SEM are shown. **e.** POMHEX selectively induces cell death against *ENO1*-deleted cells. Each data point represents a single biological replicate (n=4 experiments) of propidium iodide-positive cells relative to CT in *ENO1*-deleted (D423, red), *ENO1*-isogenically rescued (D423 *ENO1*, blue), and *ENO1*-WT (LN319, grey) cells. **f.** D423 *ENO1*-null and D423 *ENO1*-rescued glioma cells were treated with HEX (orange bars, 200 μM) and POMHEX (red bars, 78 nM). Cells were treated for 8 hours and ATP was measured with the cell titer glow assay. Individual data points and the mean ± S.E.M. of n = 12, 6 (CT) and n = 6 (HEX, POMHEX) biological replicates are shown. Significant differences are indicated, using 1-way ANOVA with Tukey's Multiple Comparison Test. ****P*<0.001. **g,h:** The effect of HEX and POMHEX on glycolytic flux was quantified by extracellular acidification rates (ECAR) in *ENO1*-null (D423, red bars) and isogenic *ENO1*-rescued cells (D423 *ENO1*, blue bars). Individual data points and the mean ± S.D. of n = 7 (CT) but n=3 for *ENO1*-rescued cells (CT) in **g** and n= 4 (HEX, POMHEX treated) biological replicates are shown. Significant differences are indicated, ****P*<0.001 ANOVA with Tukey's Multiple Comparison Test.

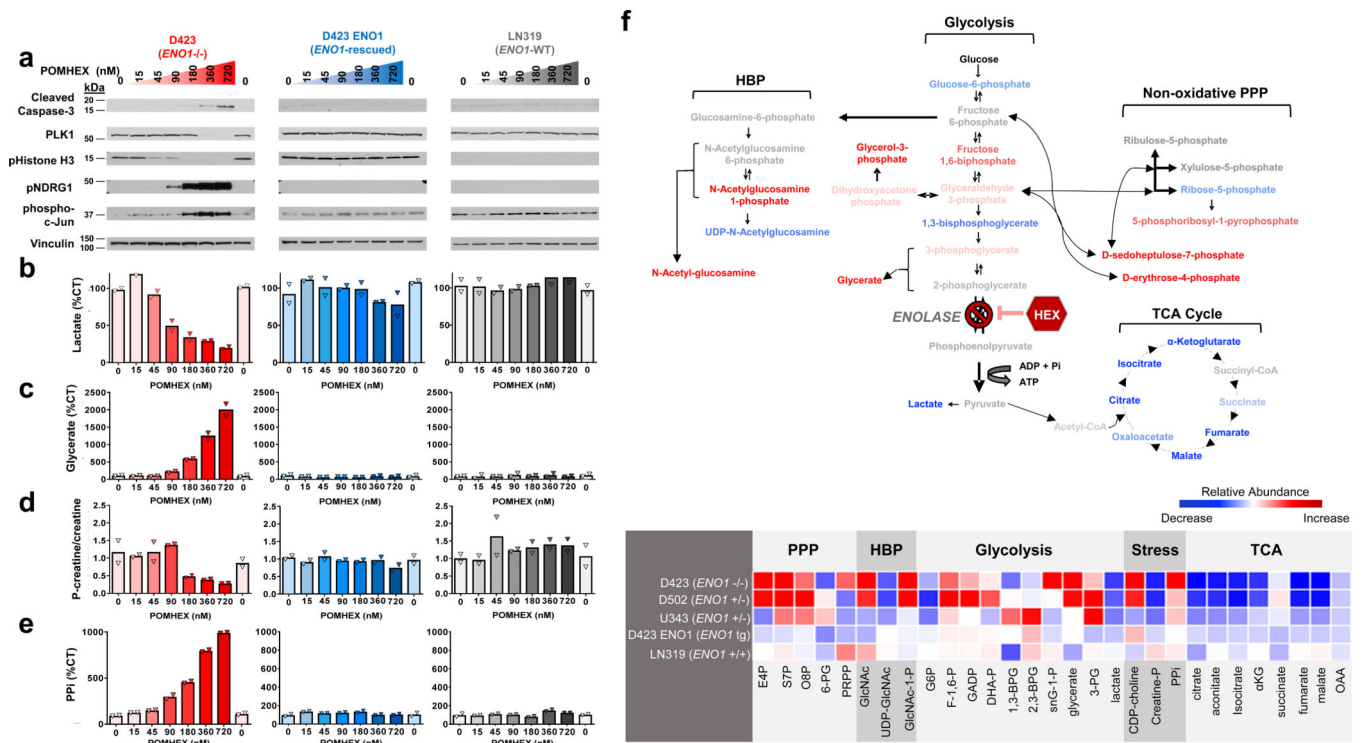


Figure 3. POMHEX selectively induces energy stress, inhibits proliferation, and triggers apoptosis in *ENO1*-deleted glioma cells. *ENO1*-deleted (D423, red), *ENO1*-isogenically rescued (D423 *ENO1*, blue), and *ENO1*-WT (LN319, grey) glioma cells were treated with the Enolase inhibitor POMHEX for 72 hours. Cells were harvested for protein lysates and polar metabolites. **a.** *ENO1*-deleted cells experience dose-dependent increase in stress response markers (phosphorylated T346 NDRG1, S73 c-Jun), decrease in proliferation (phosphorylated Histone H3, PLK1), and increase in cell death (cleaved caspase-3), as indicated by western blot. Such effects are exclusive to *ENO1*-deleted cells (left, red) and are absent in *ENO1*-WT cells (middle, blue; right, grey). **b.** Lactate levels were measured by ¹H NMR with the integral of 1.34 ppm doublet normalized to 3-(trimethylsilyl)propionic-2,2,3,3-d₄ acid standard and expressed as % of CT [(n=2(CT), mean of n=1 (treated biological replicates)]. A dose-dependent decrease in lactate levels is unique to *ENO1*-deleted, but not *ENO1*-WT, glioma cells. **c.** Glycerate levels were used as a marker of Enolase inhibition and were measured by mass spectrometry. Values are expressed as % of CT [(n=4(CT), mean of n=2 (treated biological replicates)]. A dose-dependent increase in glycerate levels was observed in *ENO1*-deleted but not *ENO1*-WT glioma cells. **d-e.** Phosphocreatine/creatinine ratio and pyrophosphate (PPI) levels quantified via mass spectrometry were used as measures of energy stress. The dose-dependent decrease in phosphocreatine to creatinine ratio (**d**) and increase in PPI (**e**) in response to POMHEX treatment is specific to *ENO1*-deleted glioma cells. Both measurements are expressed as a % of CT [N=4(CT), mean of N=2 (treated biological replicates)]. **f.** Treatment with POMHEX results in depletion of anaplerotic substrates. Top: metabolic map showing relative increases (red) and decreases (blue) of relevant metabolites in glycolysis, hexosamine biosynthesis pathway, non-oxidative pentose phosphate pathway, and TCA cycle in *ENO1*-deleted (D423) cells. Bottom: heat map of relevant metabolites in

ENO1-deleted (D423), *ENO1*-heterozygous deleted (D502, U343), and *ENO1*-WT (LN319) glioma cells. A decrease in TCA metabolites is observed across all cell lines treated with POMHEX, Relative abundance is expressed as area-under-the-curve calculations of metabolite levels obtained from dose-response POMHEX treatment.

Author Manuscript

Author Manuscript

Author Manuscript

Author Manuscript

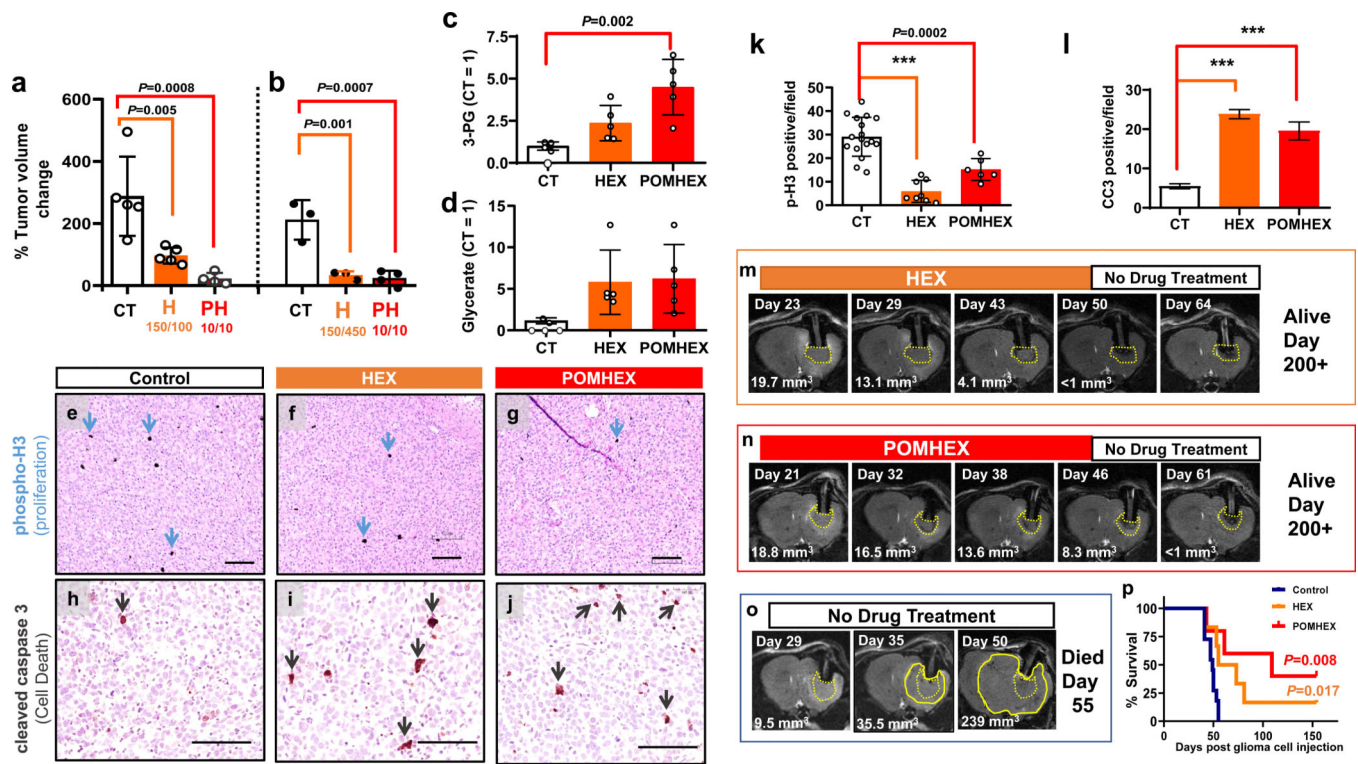


Figure 4. Target engagement and Anti-neoplastic effects of Enolase inhibitors *in vivo*.

Intracranial tumors were generated by implantation of D423 (*ENO1*-deleted) glioma cells in nude immunocompromised mice. Tumor progression was followed by T2-MRI. **a,b** Tumor volumes (mm³) and percent changes calculate in response to 1-week treatments. **a**: tumor volume changes for non-treated controls (n=5), HEX-treated (150 mpk IV + 100 mpk IP, n=5) and POMHEX-treated (10 mpk IV + 10 mpk IP, n=5) tumor bearing mice (**b**: tumor volume changes, for non-treated animals (n = 3), HEX (150 mpk IV + 450 mpk S.C., n = 3) and POMHEX (10 mpk IV + 10 mpk IP, n = 5) treated for 1-week. Animals were sacrificed after 7 day treatment for evaluation of pharmacodynamics metabolites (**c,d**) (n = 5 individual data points, see Reporting Summary) and immunohistochemistry staining (**a-d**) Mean ± S.D. are shown, One way ANOVA, with Dunnett's multiple comparison test used, *P*-values are indicated. (**e-j**). Representative images of tissue sections of HEX and POMHEX treated tumors are shown. Black size bar, 100 μm. Counts of p-H3 and CC3 positive cells per 100X section are summarized in **k** and **l**. Markers of proliferation (phospho-H3, black stain, blue arrows, **k**) and cell death (cleaved caspase 3; Red brown stain, red arrows, **l**). (CT, HEX, POMHEX n= 17, 8, 6 and n= 47, 33, 27 fields, mean ± S.E.M.). Brown-Forsythe and Welch ANOVA, and Uri-Wiggins multiple comparisons test, with individual variance was used Adjusted *P*<0.0001; is indicated as ***). Tumor formation was also followed by T2-MRI in the with long term treatments (**m-o**). While tumor growth inexorably increases in non-treated controls (**o**), treatment with HEX (75 mg/kg IV and 75 mg/kg IP, **m**) or POMHEX (10 mg/kg IV + 10 mg/kg IP per day, **n**) yielded tumor regression to the point of negligibility (Day 50). After treatment discontinuation, animals were effectively cured; tumors did not recur. **p**. Tumor-free survival curves, with long term survivors censored after 150 days.

POMHEX and HEX survival curves are compared to control. *P* values for Kaplan Mayer, with Log-rank (Mantel-Cox) test analysis are indicated.

Author Manuscript

Author Manuscript

Author Manuscript

Author Manuscript

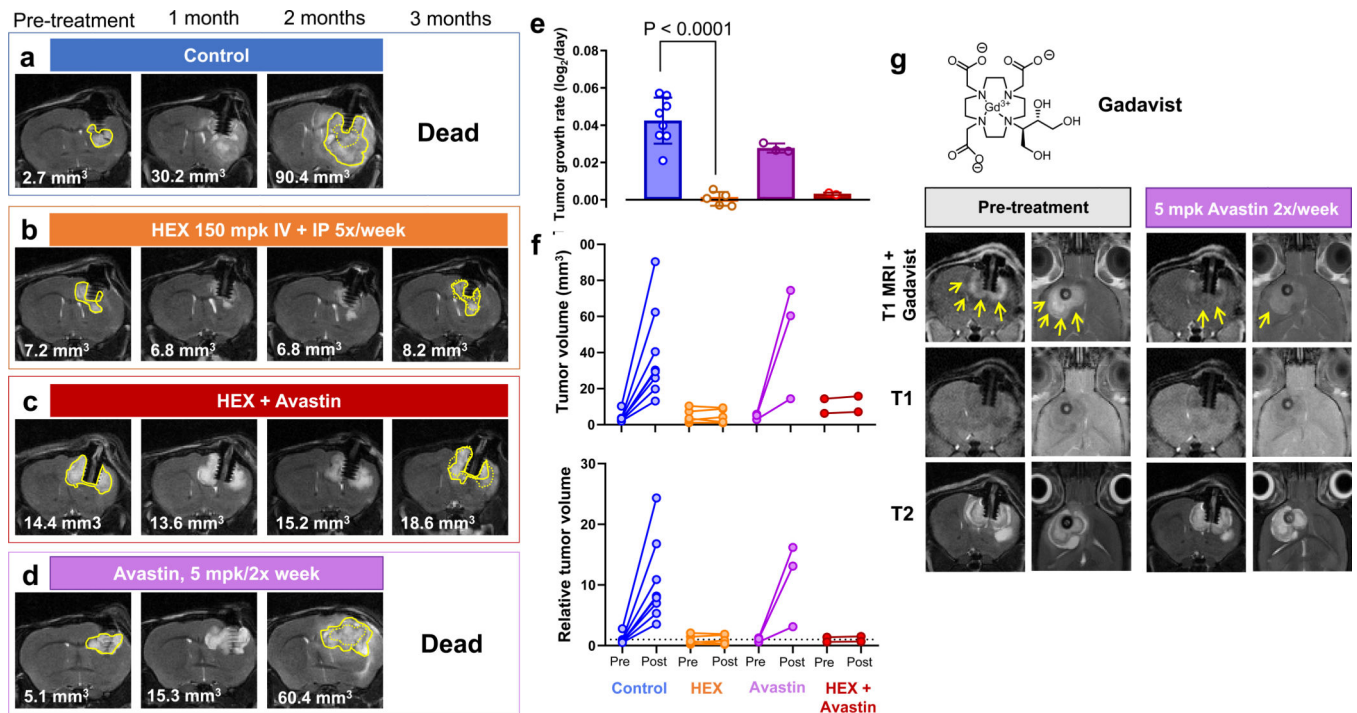


Figure 5. Efficacy of the phosphonate Enolase inhibitor HEX is not dependent on a breached blood brain barrier.

Intracranial tumors were generated by implantation of Gli56 (ENO1-deleted) glioma cells in NSG immunocompromised mice and tumor formation was followed by T2-MRI. Tumor volume changes were calculated from stacked images (mm^3) for **a** vehicle-treated controls, **b** HEX-treated (150 mpk IV + 150 mpk IP, 5 times/week), **c** Avastin + HEX, and **d** Avastin treated (5 mg/kg IP, twice per week). **e**. Intracranial tumor growth rates, (Mean \pm SD), with Brown-Forsythe and Welch ANOVA with Tamhane's T2 multiple comparisons test with individual variances $P < 0.0001$ for the effect of HEX. **f**. Tumor volumes pre- and 2 months post-treated with HEX and Avastin as indicated. Each trace represents one mouse. **g**. Gli56 intracranial tumors have extensive breach of the blood brain barrier, as shown by dramatic T1-MRI contrast enhancement upon IV injection with negatively charged, tissue impermeable, GADAVIST (yellow arrows). Treatment with Avastin (5 mg/kg twice per week) for 1 week resulted in near complete loss of T1-contrast enhancement, demonstrating restoration of the breached blood brain barrier. Tumor volume itself, as measured by T2-MRI, was minimally altered by Avastin treatment.

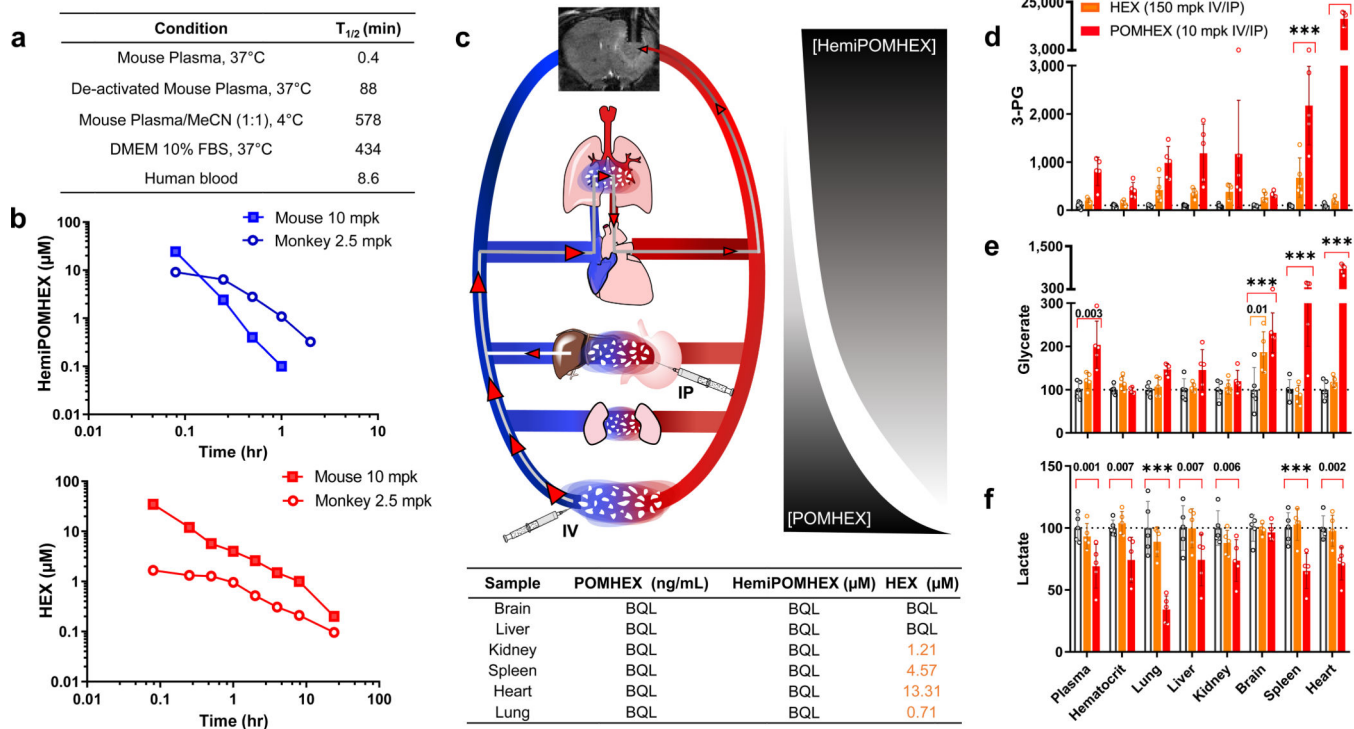


Figure 6. *Ex-vivo* and *in vivo* pharmacology of HEX and POMHEX.

a. High levels of carboxylesterase in *ex vivo* mouse plasma results in rapid hydrolysis of the first POM pro-drug group. Lower levels of carboxylesterase in human blood results in a longer half-life of POMHEX. In contrast, in cell culture media DMEM with 10% heat inactivated fetal bovine serum (FBS), POMHEX is reasonably stable, explaining the excellent *in vitro* potency. **b.** Dramatically higher drug exposure in non-human primates as compared to mice following IV injections of POMHEX. Mice (n=3; pooled) and monkeys (n=3; pooled) were injected IV with POMHEX at 10 mg/kg and 2.5 mg/kg, respectively. The lower dose in monkey was in anticipation of potentially higher toxicity (which did not materialize). POMHEX was undetectable (<50 nM) even at the earliest time point, in both monkey and mouse experiments; at 98 nM, POMHEX was detectable 1-minute post-injection, but at no time thereafter. The half-lives of HemiPOMHEX and HEX are both longer in monkey (open circles) compared to mouse (shaded circles). HEX and HemiPOMHEX were not measured at doses higher than 10 mg/kg due to the hazards associated with the derivatization agent, trimethylsilyl-diazomethane. **c.** Schematic of POMHEX in circulation when administered IP or IV in mice. Due to high levels of plasma carboxylesterase, a gradient decrease in POMHEX away from the site of injection is accompanied by a concurrent increase in HemiPOMHEX. **d-f.** Pharmacodynamic markers of Enolase inhibition in tissues of mice treated with HEX and POMHEX. Nude mice (n = 5 animals) were injected with POMHEX (10 mpk IV + 10 mpk IP; red), HEX (150 mpk IV + 150 mpk IP, orange) or DMSO (grey). After a 1-week treatment, animals were sacrificed, exsanguinated with organs flash frozen for metabolomic profiling. Key polar metabolites are expressed relative to a DMSO control. Treatment with HEX resulted in minimal Enolase inhibition, POMHEX treatment resulted in substantial Enolase inhibition, as indicated by

significant increases in 3-PG and glycerate and a decrease in lactate. Two-way ANOVA with Bonferroni's multiple comparison test used, adjusted *P* values are shown and indicated as *** if <0.001 .

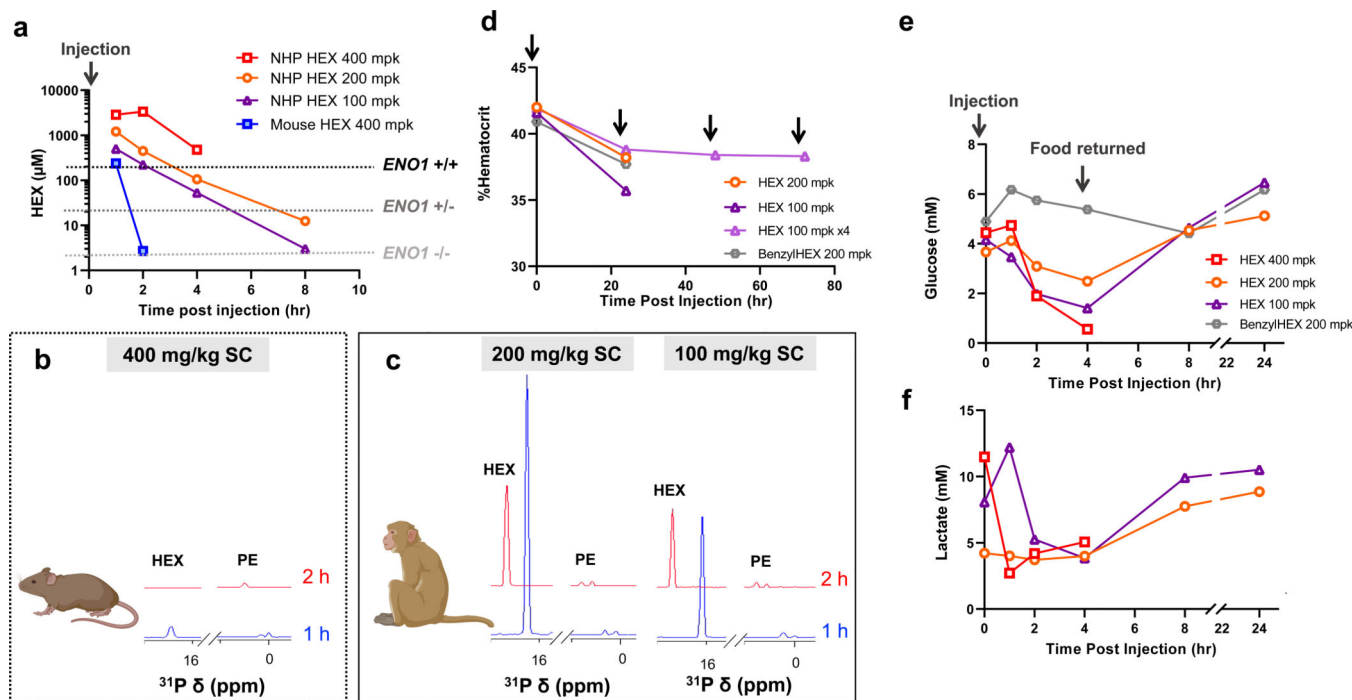


Figure 7. Plasma exposure of HEX is dramatically higher in NHP compared to mice.

a, b, c Animals were fasted overnight and injected with a single dose of HEX SC. Plasma concentrations of HEX were measured by ^1H - ^{31}P HSQC (NS = 128) with a detection limit of $>1 \mu\text{M}$. In mice, even at a dose of 400 mg/kg, HEX became undetectable 2 h post-injection (blue). In contrast, the same dose yielded plasma concentrations of $>2,000 \mu\text{M}$ in NHP over several hours. Approximate *in vitro* IC_{50} for $ENO1$ -deleted and $ENO1$ -intact glioma cells are indicated (dashed lines). **b, c**. 1D ^{31}P spectral projections from ^1H - ^{31}P HSQC NMR of either mouse (**b**) or NHP (**c**) plasma taken at 1- and 2 h post-injection. HEX (δ 16 ppm) and endogenous phosphate esters used as an internal reference (PE) are indicated. **d**. Hematocrit levels remain stable even with repeated injections of HEX with no changes in body weight (3.03 vs 2.96 kg). Black arrows indicate drug injection. An initial drop is observed 24 h after HEX injection, but this is also observed with treatment of the inactive synthetic precursor, BenzylHEX, and normalizes thereafter. According to veterinarians at Charles River Laboratories, this decrease in hematocrit can be attributed to multiple blood samplings for PK studies (a, b). **e**. Glucose levels decrease in response to HEX, but not BenzylHEX, treatment. Decreased glucose levels in the fasting state are most parsimoniously explained by Enolase inhibition in liver and kidney, which attenuate gluconeogenesis. These levels recover when food is returned, and HEX is washed out. **f**. Decreases in lactate levels in response to HEX treatment concur with overall glycolysis inhibition.